Eindhoven University of Technology

MASTER

Design of a low phase noise I/Q LC oscillator

van de Ven, Pepijn W.J.

Award date:
2000

Link to publication

Disclaimer
This document contains a student thesis (bachelor's or master's), as authored by a student at Eindhoven University of Technology. Student theses are made available in the TU/e repository upon obtaining the required degree. The grade received is not published on the document as presented in the repository. The required complexity or quality of research of student theses may vary by program, and the required minimum study period may vary in duration.

General rights
Copyright and moral rights for the publications made accessible in the public portal are retained by the authors and/or other copyright owners and it is a condition of accessing publications that users recognise and abide by the legal requirements associated with these rights.

- Users may download and print one copy of any publication from the public portal for the purpose of private study or research.
- You may not further distribute the material or use it for any profit-making activity or commercial gain

Design of a low phase noise I/Q LC oscillator

P.W.J. van de Ven

Technische Universiteit Eindhoven
Bibliotheek Centraal magazijn (BMA)
HG - 1.40 tel. (040) 247/2524
Dit werk uiterlijk terugbezorgen op laatst gestempelde datum

FA 960916

©Koninklijke Philips Electronics N.V. 2000

Supervising Professor:	Professor Dr. Ir A.H.M. van Roermund Mixed-signal Micro-electronics group Department of Electronic Engineering Eindhoven University of Technology
Supervisors:	
Ir. J.D. van der Tang	Mixed-signal Micro-electronics group Department of Electronic Engineering Eindhoven University of Technology
B.Sc. C. Vaucher	Integrated Transceivers Group Philips Research Laboratories Eindhoven
Authors' address data:	P.W.J. van de Ven WAY 5.079 pepijn.van.de.ven@philips.com

©Koninklijke Philips Electronics N.V. 2000
All rights are reserved. Reproduction in whole or in part is
prohibited without the written consent of the copyright owner.

Abstract

In many state of the art receiver architectures, In-phase (I) and Quadrature (Q) signals are used. Requirements for the I/Q signals are:

- Good amplitude matching
- Good phase matching

Those requirements can be met by I/Q RC oscillators. However, many applications also demand a high Carrier-to-Noise-Ratio (CNR). In those cases it might prove useful to use an I/Q LC oscillator instead. As the quality factor of LC oscillators is normally far higher than the quality factor of RC oscillators, the CNR will normally also be far higher. However, in state of the art I/Q (and other multi-phase) LC oscillators, the quality factor of the resonator is reduced in the process of obtaining the I/Q signals.

In this project two main research goals were addressed:

- Determine the CNR reduction of multi-phase LC oscillators compared to single-phase LC oscillators.
- How can the CNR of a multi-phase LC oscillator be optimised?

During this investigation a top-down method was used: first single-phase LC oscillators were investigated to gain insight and generate a solid foundation. Then, the focus was shifted towards multi-phase LC oscillators, the underlying theory and existing architectures. Finally, a new I/Q architecture with improved CNR is presented.

Although the design of this new architecture has not yet been optimised, an improvement in CNR of about 15 dB has been realised compared to state of the art architectures.

Preface

This report is the material result of my masters project in the Philips Research Laboratories Eindhoven. As a student in electrical engineering at the Eindhoven University of Technology I have spent the last 9 months working on (I/Q) LC oscillators in the Integrated Transceivers group.

Of course I would never have come this far without the help of a few persons I would very much like to mention. First of all I would like to express my gratitude towards Johan van der Tang. Started out as my supervisor from the Natlab he transformed to my supervisor from the Eindhoven University of Technology when he started working there. I would like to thank Johan van der Tang for all the work and effort he has so willingly invested in me and this project.

Cicero Vaucher was a worthy successor of Johan van der Tang as my supervisor within the Natlab. He has been a great help in reading my report critically and in being my contact within the Philips Natlab for which I would like to thank him.

Naturally I would like to thank the people that have made this masters project possible in the first place: Prof. Dr. Ir. van Roermund as my supervising professor from the Eindhoven University of Technology and Pieter Hooijmans as the group leader from the Integrated Transceivers group.

Forced by etiquette I have to say the following at the end of this acknowledgement: I would kindly like to thank all my colleagues from the Integrated Transceivers group for having made the last 9 months a very pleasant experience.

Eindhoven, July 12th 2000.

Contents

1 Introduction

Many state of the art transceivers need In-phase (I) and Quadrature (Q) signals. In zero IF architectures, for example, I/Q signals are used to convert the RF signal directly to a baseband signal. Low IF architectures also make use of an I/Q signal path and I/Q is used in state of the art DECT and satellite receivers. Advanced Data Clock Recovery architectures (DCR), used in optical interface ICs, need I/Q signals for correct operation.

1.1 Various ways to generate I/Q signals

I/Q signals can be generated in several ways. Using a single-phase oscillator the I/Q signals can be obtained through the use of a divider-by-two circuit. In this method the oscillator is required to oscillate at a frequency equal to twice the desired I/Q signal frequency. When I/Q signals at high frequencies are desired, it may be very difficult to obtain the required oscillator frequency.

Polyphase networks are another means of generating I/Q signals. Using an RC network with limiters and again a single-phase oscillator, the I/Q signals are obtained. For good phase and amplitude matching this method requires an oscillator signal having a low harmonic distortion. This, however, contradicts with CNR requirements as the CNR increases with increasing voltage swing. To circumvent the mentioned problems there has been a growing interest for oscillators with I/Q outputs.

1.2 I/Q oscillators

RC oscillators are easy to integrate and can provide I/Q signals. Using an even amount of stages, an I/Q oscillator is obtained that is correct-by-construction. This means that, due to the Barkhausen criterion, the stages are forced to oscillate in such a way that the I/Q requirement is automatically met. Due to the fact that energy can not be stored in the RC oscillator, the quality factor of the two-stage RC oscillator equals 1. Therefore this architecture can only be used if the CNR requirement of the application isn't very tight.

When the application requires a high CNR, it might be necessary to use LC oscillators as their resonator quality factor is normally far bigger than 1. Similar to RC oscillators, LC oscillators can be used in multi-stage oscillators to obtain a correct-by-construction I/Q architecture. However, coupling the LC oscillators has a great influence on the quality factor of the resonator. This can be shown using expression 1 that relates the slope of the resonator phase transfer to the quality factor [1].

$$Q = \frac{w_{osc}}{2} \frac{\delta\phi}{\delta\omega} \tag{1}$$

The term $\frac{\delta\phi}{\delta\omega}$, and therefore Q, is maximal at zero degrees phase shift. Due to coupling

[1] In chapter 5 it will be shown that this equation is not always valid for multi-phase LC oscillators. It does however give the insight needed at this point

the LC oscillators, the oscillator stages are, however, forced to oscillate at non zero phase shifts, resulting in a degraded quality factor. For the extreme situation in which the resonator phase shift is 90°, the quality factor has even dropped to 1 in a 2-stage I/Q LC oscillator. It goes without saying that this decrease in quality factor, and thus CNR, is intolerable as the LC oscillator was used for its high CNR.

1.3 Outline of the project

The purpose of this project was to find an I/Q LC architecture that makes optimum use of the quality factor of the LC resonator. To obtain a theoretically well funded result, a top-down approach was chosen. This top-down approach is reflected in the structure of this report:

Chapter 2

Noise originating from the resonator is investigated. Approximate equations for voltage noise that are very similar to the well-known expression for CNR, called Leeson's equation, are derived and their limitations are investigated. A rule of thumb is presented to quantify boundary frequencies for the use of the approximate equations.

Chapter 3

A transistor model is introduced and its noise sources are listed. All noise sources are referred to one noise input voltage of the transistor model.

Chapter 4

The results from chapter 2 and chapter 3 are combined to arrive at an approximate expression for the total oscillator noise. Again the limitations of this approximate equation are investigated. A new figure of merit, called **Implementation Loss** is defined and used.

Chapter 5

In this chapter the discussion is shifted towards multi-phase oscillators. A new expression for the quality factor is presented and is used to derive expressions for the CNR in multi-phase LC oscillators. This CNR, that depends on the phase shift, is used to obtain a new implementation loss on behavioural level. This implementation loss is defined as the losses due to implementing the multi-phase functionality. Furthermore an onset is given towards a new architecture using explicit phase shift networks, proposed by [1].

Chapter 6

A literature study is performed to obtain insight in the status quo of multi-phase LC oscillators. The found architectures are presented and rated using a normalised CNR.

Chapter 7

As the literature study did not result in satisfactory solutions for the main problem (the decrease in quality factor), a new I/Q LC architecture is proposed that makes use of explicit phase shifts. The circuit is presented and simulations are performed to compare the new architecture to both an LC and a common I/Q LC oscillator.

Chapter 8

Finally conclusions are drawn and an outlook is given.

2 Noise in LC resonators

Calculating the total phase noise in oscillators is a complicated matter. Due to the non-linear behaviour of the oscillator, noise is upconverted from the baseband and downconverted from higher harmonics, resulting in an increase of phase noise around the oscillation frequency. In this report calculations will be performed using linear models. Although in doing so, important effects are not accounted for, this approach does give way to important insights. Non-linear phenomena in oscillators are thoroughly discussed in for example [2]. The transfer function from a noise source to the output can be a very extensive expression, making it hard to decide what to do in order to minimize the output noise power.

However, as we are mainly interested in the noise power close to the carrier frequency, it might be possible to introduce a few simplifications. This was recognised in the early sixties and in 1966, Leeson [3] was the first one to write down a simple formula approximating the power spectrum of an oscillator close to the carrier. Nowadays this expression is called Leeson's equation.

$$CNR = -10\,Log\left[\frac{F\,k\,T}{2\,P}\frac{1}{Q^2}\left(\frac{\omega_{osc}}{\Delta\omega}\right)^2\right] \tag{2}$$

with

CNR	the Carrier to Noise Ratio		dBc/Hz
F	the amplifier noise figure		
k	the Boltzmann constant,	1.3804×10^{-23}	J/K
T	the absolute temperature		K
Q	the quality factor of the resonator		
ω_{osc}	the oscillation frequency of the resonator		rad/s
$\Delta\omega$	the offset from the oscillation frequency		rad/s

2.1 Carrier to Noise Ratio, Phase Noise and Voltage Noise

The Carrier to Noise Ratio (CNR) is defined as the ratio of oscillator power at the oscillation frequency to oscillator power at a certain offset frequency, $\Delta\omega$, measured in a bandwidth of 1 Hz. The oscillator power at a certain offset frequency is referred to as oscillator phase noise. The amplifier noise figure, F, is introduced as it is very difficult to derive generic equations for the amplifier noise. This is due to the fact that amplifier noise is highly dependent on the chosen amplifier topology. A widely used strategy to determine the amplifier noise figure, is to calculate it from simulations. This, however, does not give any insight in the mechanisms that are the cause of noise in the active circuit. Therefore, it is desired to get explicit expressions for the amplifier noise figure. As, in this study, only one amplifier topology will be used, an accurate approximation of the amplifier noise, and thus the amplifier noise figure, can be obtained through the use of

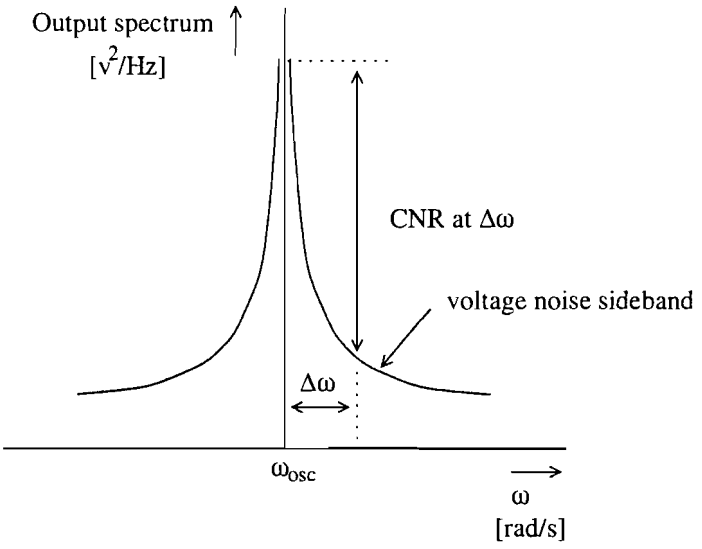

Figure 1: Definition of the Carrier to Noise Ratio

transistor models.

Over the years, formula 2 has proven to be a very useful aid in estimating the CNR of oscillators. However, as Leeson's equation is an approximation it is very important to know its limitations. In this chapter the limitations of Leeson's equation will be shown using a linear oscillator model with an ideal active circuit. I.e. the active circuit does not contribute any noise. Disadvantage of the linear model is that oscillator carrier power can not be determined from this model. The voltage swing of an oscillator is limited due to limiting in the transistors. As there is no limiting factor in the linear model, voltage swing and thus carrier power can not be calculated. Oscillator carrier power is one of the variables in Leeson's equation and thus it is impossible to verify Leeson's equation with a linear model. Therefore, this chapter will only deal with oscillator phase noise, for which an approximation based on Leeson's equation can be derived:

$$\overline{v^2_{n_{Leeson-phase}}(\omega)} = \frac{k\,T\,R_p}{2}\,\frac{1}{{Q_p}^2}\left(\frac{\omega_{osc}}{\Delta\omega}\right)^2 \tag{3}$$

Equation 3 describes the phase noise around the oscillation frequency. However, this phase noise is only part of the oscillator noise. As described in [4] total noise power, or voltage noise power, is equally shared between AM and PM, which is equivalent to respectively amplitude noise and phase noise. Thus, the voltage noise power is twice the phase noise power:

$$\overline{v^2_{n_{Leeson-voltage}}(\omega)} = k\,T\,R_p\frac{1}{{Q_p}^2}\left(\frac{\omega_{osc}}{\Delta\omega}\right)^2 \tag{4}$$

In section 2.2 a physical resonator will be examined, resulting in analytical expressions for the output voltage noise power resulting from the resonator, the oscillation frequency and the transconductance, g_m, necessary to compensate the losses in the tank in order to

sustain oscillation. These expressions have been verified through simulations. Section 2.3 shows how equation 4 can be derived and describes the approximations applied to obtain this equation. Then the errors, due to the approximations are calculated and in section 2.4 a rule of thumb is derived for the maximum offset frequency for which the approximate equation can be used without making an excessive error. Finally, in section 2.5 conclusions are drawn.

2.2 Noise in series resistance resonators

As shown in figure 2, a non ideal LC resonator can be represented by an ideal capacitor and an ideal inductor, both in series with a resistor.

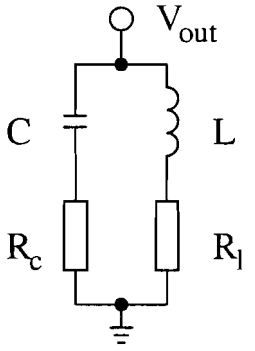

Figure 2: Circuit diagram of an LC resonator circuit

The two resistors are noisy elements, contributing to the total output noise power. To model the resistors' contribution to the total noise of the oscillator, a noise current source is placed in parallel with each resistor, as shown in figure 3.

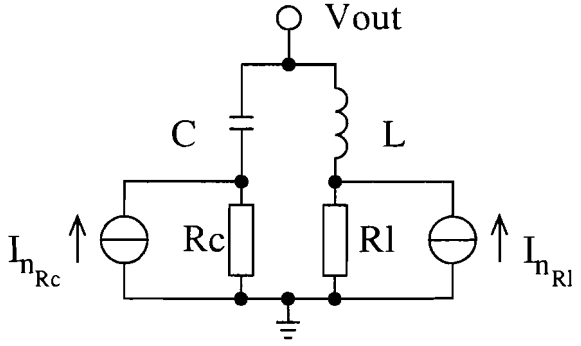

Figure 3: Equivalent circuit of LC resonator with noisy resistors

The value of the current, $i_{n_{R_x}}$, is related to R_x:

$$i_{n_{R_x}} = \sqrt{\frac{4\,k\,T\,B}{R_x}} \tag{5}$$

with: B, the bandwidth of the system with which the noise is measured.

The noise current sources from the resistors result in a mean squared noise voltage across the resonator. Using the equivalent circuit diagram of figure 3 this mean squared noise voltage can be calculated. In equation 6 the noise bandwidth, B, has been chosen as 1 Hz.

$$\overline{v^2_{n_{resonator}}} = 4kT \cdot \frac{\left(R_l + C^2 R_c{}^2 R_l \omega^2 + C^2 Rc R_l{}^2 \omega^2 + C^2 L^2 R_c \omega^4\right)}{1 - 2CL\omega^2 + C^2\omega^2\left(R_c{}^2 + 2R_c R_l + R_l{}^2 + L^2\omega^2\right)} \quad (6)$$

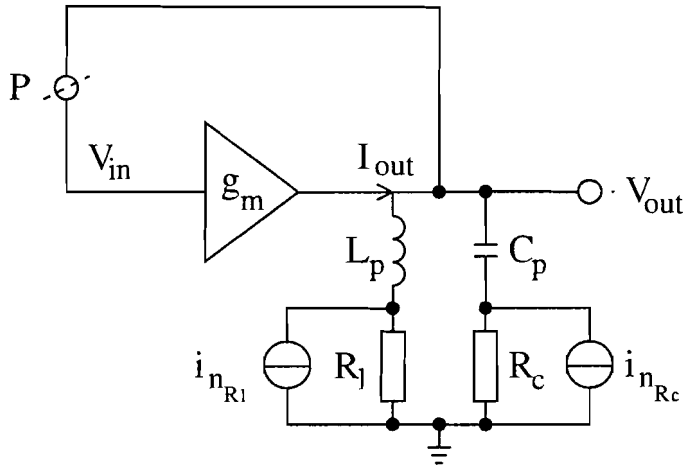

Figure 4: Simple model of an oscillator with noisy resonator

Figure 4 shows a simple feedback model of an oscillator. Now the contribution of the resonator to the oscillator noise is known, the noise can be transferred to the input of this feedback model. Cutting the feedback loop open at point P, the open loop transfer function can be calculated to be:

$$H(j\omega)\Big|_{\text{open loop}} = \frac{V_{out}}{V_{in}}\Big|_{\text{open loop}} = g_m Z_o \quad (7)$$

with Z_o the impedance of the LC resonator equal to:

$$Z_o = \frac{(L + C R_c R_l)\,\omega + j\left(C L R_c \omega^2 - R_l\right)}{C\,(R_c + R_l)\,\omega + j\left(C L \omega^2 - 1\right)} \quad (8)$$

and g_m the transconductance of the amplifier. To obtain expressions for the oscillation frequency and the transconductance, the Barkhausen criterion [2] [5] has to be applied:

[2]Note that in order for the oscillator to start up, $|H(j\omega)_{openloop}|$ has to be greater than 1

$$\begin{aligned} |H(j\omega)|\Big|_{\text{open loop}} &= 1 \\ \angle H(j\omega)\Big|_{\text{open loop}} &= 0 \end{aligned} \tag{9}$$

From equation 7 and equation 9 it follows that in steady state the transconductance is equal to the conductance of the LC resonator at the oscillation frequency, ω_{osc}. In that case g_m will exactly compensate the losses due to the real part of the resonator impedance. In case of the situation depicted in figure 4, the phase condition of the Barkhausen criterion implies that at the oscillation frequency, the imaginary part of the resonator impedance is zero. Therefore the oscillation frequency [3] (eq. 10) can be calculated by solving $Im[Z_o] = 0$ for ω. Substituting the found expression for ω_{osc} into Z_o gives the resonator impedance at the oscillation frequency, and thus g_m (eq. 11).

$$\omega_{osc} = \frac{\sqrt{L - C\,R_l^2}}{\sqrt{L\,C}\sqrt{L - C\,R_c^2}} \tag{10}$$

$$g_m = \frac{C\,(R_c + R_l)}{L + C\,R_c\,R_l} \tag{11}$$

Now both Z_o and g_m are known the input mean squared noise voltage can be calculated. Dividing $\overline{v_{n_{resonator}}^2}$ by the squared modulus of equation 7, $|g_m\,Z_o|^2$, the input mean squared noise voltage is obtained:

$$\begin{aligned} \overline{v_{n_{in}}^2(\omega)} = {} & 4\,k\,T\,(L + C\,R_c\,R_l)^2 \cdot \\ & \frac{\left(R_l + C^2\,R_c^2\,R_l\,\omega^2 + C^2\,R_c\,R_l^2\,\omega^2 + C^2\,L^2\,R_c\,\omega^4\right)}{C^2\,(R_c + R_l)^2\,\left(R_l^2 + L^2\,\omega^2\right)\left(1 + C^2\,R_c^2\,\omega^2\right)} \end{aligned} \tag{12}$$

Now the closed loop output mean squared noise voltage can be obtained by multiplying the mean squared input noise voltage, $\overline{v_{n_{in}}^2(\omega)}$, by the **closed** loop transfer function.

$$\overline{v_{n_{out}}^2(\omega)} = \overline{v_{n_{in}}^2(\omega)} \cdot |H(j\omega)|^2\Big|_{\text{closed loop}} \tag{13}$$

Using figure 4 the closed loop transfer function $H(j\omega)\,|_{closed\,loop}$ can be derived:

$$H(j\omega)\Big|_{\text{closed loop}} = \frac{V_{out}}{V_{in}}\Big|_{\text{closed loop}} = \frac{g_m\,Z_o}{1 - g_m\,Z_o} \tag{14}$$

Substituting the equations for Z_o (eq. 8) and g_m (eq. 11) in equation 14 and substituting the result together with equation 12 in equation 13 yields:

[3] In appendix A the dependency of the oscillation frequency on the resonator quality factors is discussed

$$\overline{v_{n_{out}}^2(\omega)} = 4kT\,(L + C\,R_c\,R_l)^2 \cdot \frac{\left(R_l + C^2\,R_c{}^2\,R_l\,\omega^2 + C^2\,R_c\,R_l{}^2\,\omega^2 + C^2\,L^2\,R_c\,\omega^4\right)}{\left(L - C\,R_l{}^2 - C\,L^2\,\omega^2 + C^2\,L\,R_c{}^2\,\omega^2\right)^2} \quad (15)$$

To verify the derived formula for $\overline{v_{n_{out}}^2(\omega)}$, the oscillator model can be simulated. In Pstar the resonator circuit has been modelled and a noise analysis at a centre frequency of 1 GHz has been performed (see appendix B). Figure 5 shows the results of this simulation in which NMSV is the by the simulator calculated mean square noise voltage. The difference between $\overline{v_{n_{out}}^2(\omega)}$ and the simulated mean squared output noise voltage is less than 0.6 percent which can be ascribed to the finite numerical accuracy. Also for $\omega \rightarrow 0$ and $\omega \rightarrow \infty$ equation 15 matches the simulated mean squared noise voltage.

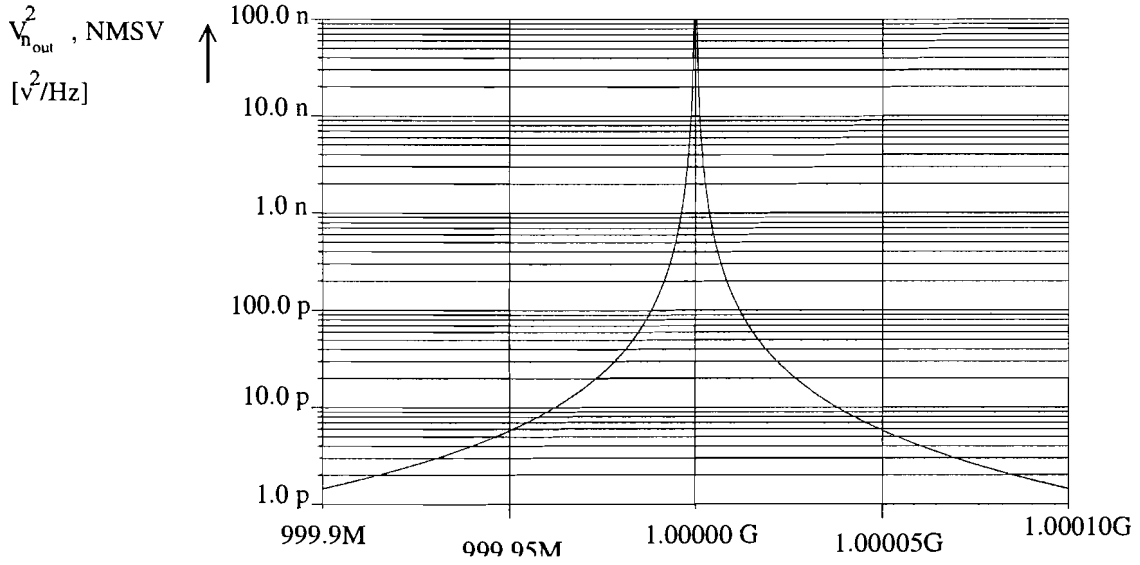

Figure 5: Graph of calculated, $\overline{V_{n_{out}}^2}$, and simulated, NMSV, mean squared noise voltages

2.3 An approximate equation for resonator noise

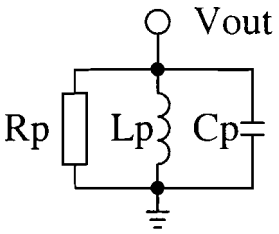

Figure 6: Representation of LC resonator with all losses modelled in one resistor

Alternatively $\overline{v_{n_{out}}^2(\omega)}$ can be calculated using the resonator model shown in figure 6. Using series to parallel network transformations, the resonator from figure 2 can be represented by the resonator from figure 6 with:

$$R_p(\omega) = \frac{R_c\left(1+Q_c(\omega)^2\right) R_l \left(1+Q_i(\omega)^2\right)}{R_c\left(1+Q_c(\omega)^2\right) + R_l\left(1+Q_i(\omega)^2\right)} \tag{16}$$

$$L_p(\omega) = L\frac{1+Q_i(\omega)^2}{Q_i(\omega)^2} \tag{17}$$

$$C_p(\omega) = C\frac{Q_c(\omega)^2}{1+Q_c(\omega)^2} \tag{18}$$

Q_i and Q_c in equations 16 through 18 are respectively the quality factor of an inductor, L, with series resistance, R_l, and a capacitor, C, with series resistance, R_c.

$$Q_i = \frac{\omega L}{R_l}, \qquad Q_c = \frac{1}{\omega C R_c} \tag{19}$$

As shown in Appendix C, the output noise due to this resonator equals:

$$\overline{v_{n_{out-alt}}^2(\omega)} = 4kT R_p \frac{1}{\left(1-gm R_p\right)^2 + (\upsilon Q_p)^2} \tag{20}$$

with

$$Q_p(\omega) = R_p(\omega)\sqrt{\frac{C_p(\omega)}{L_p(\omega)}} \tag{21}$$

and

$$\upsilon = \frac{\omega}{\omega_0(\omega)} - \frac{\omega_0(\omega)}{\omega} \tag{22}$$

with $\omega_0(\omega)$ the oscillation frequency of the parallel resonator, which is equal to $\frac{1}{\sqrt{L_p(\omega)\,C_p(\omega)}}$. As the transformations used are no approximations whatsoever, equation 20 is equivalent to equation 15.

2.3.1 Approximating $\omega_0(\omega)$, $R_p(\omega)$, $Q_p(\omega)$ and $v(\omega)$

Comparing equation 20 with the Leeson like equation for voltage noise (eq. 3) it should be noted that both equations are quite similar. In fact, Leeson's equation is an approximate version of equation 20. The difference between both equations is that in Leeson's equation all frequency dependent terms have been approximated by their value at the oscillation frequency, ω_{osc}. Therefore Leeson's equation can be derived from equation 20 by defining $\omega = \omega_{osc} + \Delta\omega$ and assuming that $\Delta\omega << \omega_{osc}$. In this case v can be approximated by $\frac{2\Delta\omega}{\omega_0}$ and the value of the terms ω_0, R_p and Q_p can be assumed to be independent of ω and equal to:

$$\begin{aligned} \omega_{00} &= \omega_0(\omega)|_{\omega=\omega_{osc}} &&= \omega_{osc} \\ R_{p0} &= R_p(\omega)|_{\omega=\omega_{osc}} &&= 1/gm \\ Q_{p0} &= Q_p(\omega)|_{\omega=\omega_{osc}} \end{aligned}$$

Using those assumptions in equation 20 yields:

$$\overline{v^2_{n_{Leeson-voltage}}(\omega)} = k\ T\ R_{p0}\frac{1}{{Q_{p0}}^2}\left(\frac{\omega_{osc}}{\Delta\omega}\right)^2 \tag{23}$$

Equation 23 is equal to the Leeson-like equation introduced at the beginning of this chapter, equation 4.

2.3.2 Errors introduced by approximating $\omega_0(\omega)$, $R_p(\omega)$, $Q_p(\omega)$ and $v(\omega)$

Figure 7 shows the error due to the approximations in equation 23. This error is defined as:

$$Error_{leeson} = 10^{10}Log(\frac{NMSV}{v^2_{n_{Leeson-voltage}}}) \tag{24}$$

thus giving the error relative to the simulation result, NMSV, in dB.

To investigate the error made by assuming $v = \frac{2\Delta\omega}{\omega_0}$, $\overline{v^2_{n_{out-fixed}}(\omega)}$ is defined as:

$$\overline{v^2_{n_{out-fixed}}(\omega)} = k\ T\ R_{p0}\frac{1}{Q_{p0}\,v^2} \tag{25}$$

As the only difference between equation 23 and 25 is that v has not been approximated in equation 25, equation 25 can be used to show the error made by approximating v. Therefore $Error_{fixed}$ is defined as:

$$Error_{fixed} = 10^{10} Log\left(\frac{NMSV}{v^2_{n_{out-fixed}}}\right) \tag{26}$$

$Error_{fixed}$ is shown in figure 7 as well. As expected both error functions have about the same value for $f \approx f_{osc}$[4].

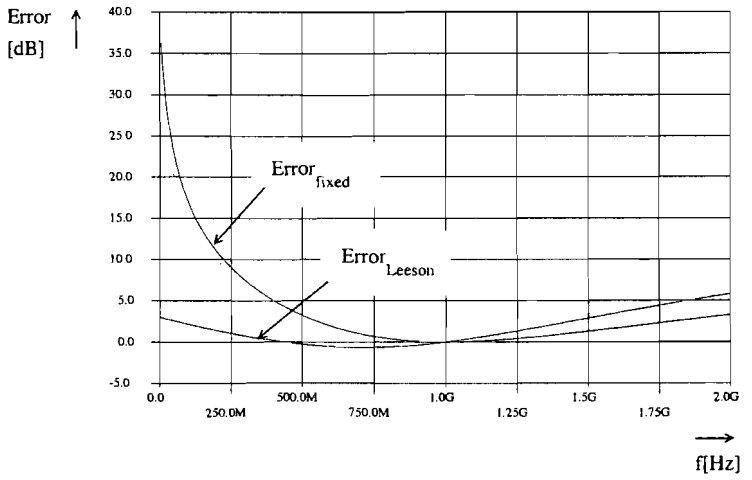

Figure 7: The error made by approximating the component values, i.e. $Error_{fixed}$, and the error made by also approximating v, i.e. $Error_{Leeson}$, for $f_{osc} = 1\,GHz$ and $Q_{po} = 25$

2.4 Boundary frequencies for use of the approximate equations; a rule of thumb

The Leeson like approximation for voltage noise (eq. 23) gives more insight in the way the noise depends on factors like the quality factor of the resonator and the offset frequency than the exact formula (eq. 20). Therefore it would be very convenient if the latter could be replaced by the former. In order to be able to do so, one has to investigate whether the error made by approximating the exact equation is acceptable.

From figure 7 it is obvious that for a certain frequency band around f_{osc}, $Error_{leeson}$ is close to 0 dB. This error function can also be expressed in an analytical way as:

$$Error_{leeson} = 10^{10} Log\left(\frac{\overline{v^2_{n_{out-alt}}(f)}}{v^2_{n_{Leeson-voltage}}}\right)$$

[4]Expressing noise as a function of the frequency in Hz, is of course equivalent to expressing noise as a function of the angular frequency in $\frac{rad}{s}$

$$= 10^{10} Log \left(\frac{4\,k\,T\,R_p \frac{1}{(1-gm\,R_p)^2+(Q_p\,v)^2}}{k\,T\,R_{p0} \frac{1}{Q_{p0}{}^2} \left(\frac{f_{osc}}{\Delta f}\right)^2} \right)$$

$$= 10^{10} Log \left(\frac{R_p\,Q_{p0}^2\,\Delta f^2}{((1-g_m\,R_p)^2 + (v\,Q_p)^2)\,R_{p0}\,f_{osc}^2} \right) \quad (27)$$

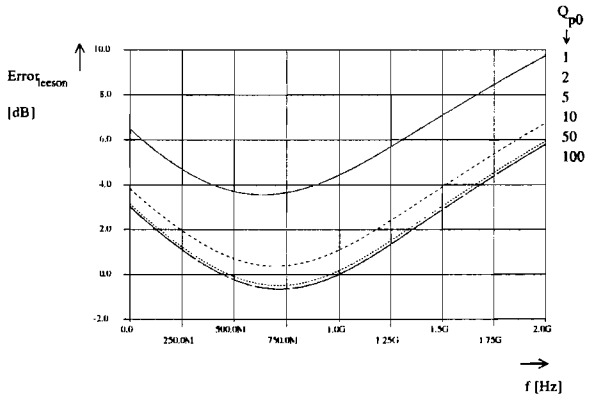

(a) $Error_{leeson}$ for several values of the resonator quality factor, Q_{p0}

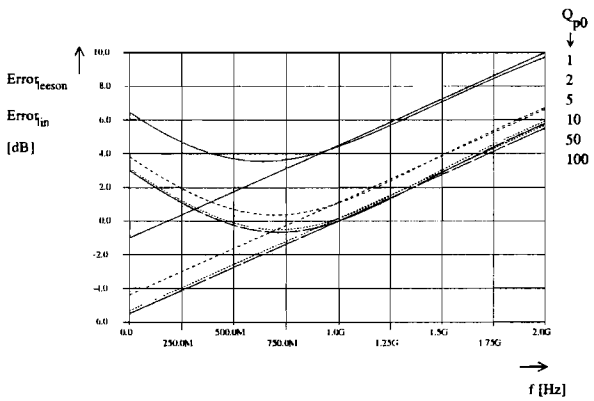

(b) $Error_{leeson}$ with it's approximation, $Error_{lin}$

Figure 8: Linearisation of the error introduced due to using the Leeson-like approximation, $\overline{v_{n\,Leeson-voltage}^2}$

Figure 8 shows a plot of this error versus the frequency offset, Δf. From the graphs it can be seen that for frequencies higher than f_{osc} the error can be linearised by the line:

$$Error_{lin} = \frac{4.5}{Q_{p0}^2} + 5.5\frac{\Delta f}{f_{osc}} \tag{28}$$

The linearised error function, $Error_{lin}$ makes it possible to obtain expressions for a certain Δf_{max}, the largest offset from the carrier frequency, for which the approximate voltage noise equation, (eq. 23), can still be used without introducing significant errors. As the measurement accuracy is of the order of ± 1 dB, the error due to using this equation is also permitted to be ± 1 dB. From figure 8 it can be seen that the error never exceeds -1 dB. Therefore, one does only have to define an upper limit for the maximum permitted frequency offset[5]. Combining the maximum allowed error of +1 dB with equation 28 and solving for Δf yields:

$$\Delta f_{max} = \left(1 - \frac{4.5}{Q_{p0}^2}\right) \cdot \frac{f_{osc}}{5.5} \tag{29}$$

Figure 8 shows that equation 29 should result in a positive value for Δf. If this is not true, the error function does not come within the ± 1 dB band at all. Taking e.g. Q_{p0} to be 1, Δf_{max} is calculated to be -0.64 $\cdot$ f_{osc}. This value is negative and thus the error is always greater than 1 dB, as can also be seen from figure 8.

Q_{p0}	Calculated Δf_{Max} [MHz]	Measured Δf_{Max} [MHz]	Error @ f_{osc} [dB]
1	-636	—	4.44
2	-22.7	—	1.09
3	91	107	0.49
4	131	147	0.28
5	149	163	0.18
6	159	173	0.13
7	165	179	0.10
8	169	183	0.07
9	172	185	0.06
10	174	187	0.05
20	180	193	0.017
50	181	193	0.008
100	182	193	0.007

Table 1: Measured and simulated maximum offset frequencies; f_{osc} = 1 GHz

Table 1 shows a list of maximum offset frequencies for several values of the quality factor, Q_{p0}, and an oscillation frequency of 1 GHz. Both the measured value and the from the rule of thumb (eq. 29) calculated value are displayed. It can be seen that the calculated maximum offset frequency is smaller than the measured one. Equation 29 can thus be used as a rule of thumb to estimate a safe value for the maximum offset frequency at which the approximate voltage noise equation can still be used without introducing unacceptable errors.

[5]The lower limit is chosen to be equal to the upper limit

2.5 Conclusions

In this chapter the mean squared output noise voltage of a resonator with an ideal transconductance was derived, both for a resonator with series resistances and for a resonator with a parallel resistance. Through network transformations the series resistances can be described with a frequency dependent parallel resistance, making the expressions for mean squared output noise for both resonators equivalent. Using the resonator with a parallel resistance, an approximation for the voltage noise, and thus the phase noise, has been deduced together with a rule of thumb that can be used to determine a safe estimate for the frequency band in which the Leeson-like approximation is accurate.

3 Noise in the active circuit

Up until now the active part of the oscillator was regarded to be noiseless. In real oscillators however, the active part contributes significantly to the total output noise. In this chapter the contribution is calculated. While the contribution of the resonator part of the oscillator to the total noise solely exists of (shaped) thermal noise, the active part of the oscillator contributes three kinds of noise: thermal noise, shot noise and 1/f noise. In section 3.1 the transistor model is introduced. A brief overview of noise in bipolar transistors is given in section 3.2. These noise sources are added to the model in section 3.3 and are referred back to the input of the open loop system in section 3.4. Analogous to the strategy used in chapter 2, the open loop input noise is referred to a closed loop input noise in section 3.5. Finally, in section 3.6, the results are listed.

3.1 Modelling the active circuit

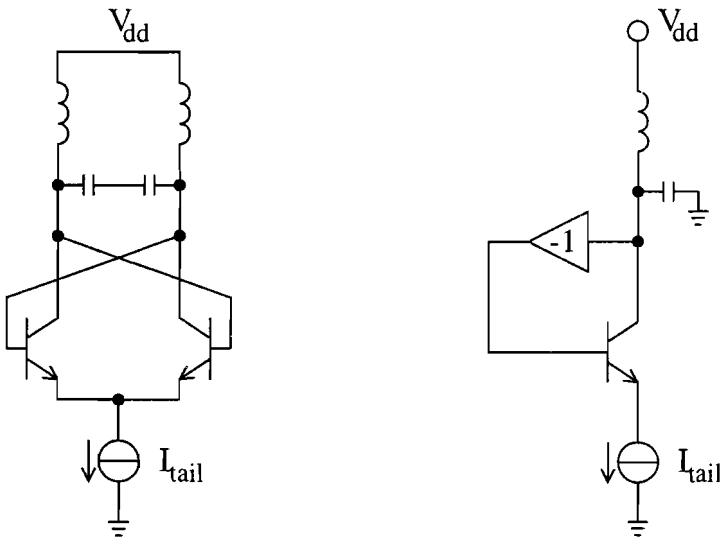

(a) Cross coupled pair LC oscillator

(b) Single ended LC oscillator

Figure 9: Circuit diagram of the used oscillator

The active part, as shown in figure 9a consists of two bipolar NPN-transistors forming a differential amplifier. As both transistors contribute the same amount of noise to the total noise and those contributions are uncorrelated, the noise calculations can be simplified to a noise analysis for one transistor. The noise due to both transistors will then equal twice the calculated noise. In the single ended model, figure 9b, the feedback has to be the same as the feedback in the differential amplifier. As this feedback is negative, an inverter has to be put in the feedback path of the single ended amplifier.

For modelling, the hybrid π model, shown in figure 10 will be used. In this model the resistance R_b is due to the resistance from the external base to the internal base. R_π models the dc base current. C_π is due to the capacitance between the internal base and the emitter. This capacitance consists of a base charging capacitance and a base-emitter depletion layer capacitance. Between the collector and the substrate a capacitance, C_{cs}, due to the collector-substrate junction is present. As the emitter of the transistors in the differential amplifier is a virtual ground and the substrate is connected to ground, C_{cs} can be seen as connected between the collector and the emitter. Finally the voltage controlled current source, I_c, represents the collector current due to the induced voltage on the internal base. To incorporate the inverter (see figure 9b), one can simply invert the direction of the collector current. To make future calculations easier, the capacitance from the internal base to the collector, C_μ, can be approximated by two Miller capacitances [6].

$$\begin{aligned} C_{M1} &= (1 + g_f Z_{ce}) C_\mu \\ C_{M2} &= (1 + \frac{1}{g_f Z_{ce}}) C_\mu \end{aligned} \tag{30}$$

with C_{M1} and C_{M2} as presented in figure 10. Z_{ce} is equal to the impedance observed between the collector and the emitter (including the impedance due to the resonator but of course without C_{M2}) and g_f is the transconductance of the transistor ($g_f \approx 40\, I_c$).

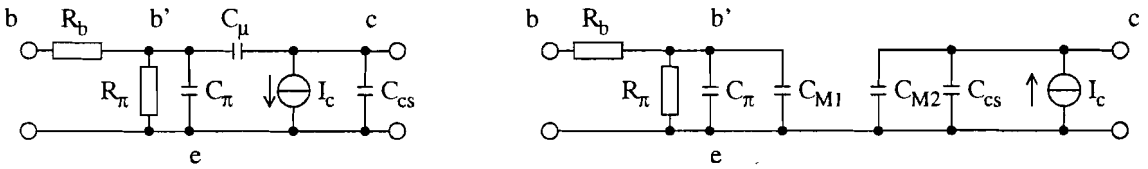

(a) Hybrid π model

(b) Hybrid π model with inverted collector current and Miller capacitances

Figure 10: Circuit diagram of the hybrid π model

3.2 Noise in a transistor

As stated, the active part of the oscillator adds three types of noise to the total noise.

Shot noise arises from the fact that the amount, N, of carriers crossing a bipolar pn junction, is a statistically varying amount. As the collector current is equal to $\frac{N\,q}{t}$, the collector current shows the same statistical variation. Due to the division of the emitter current in base and collector current, the base current also contains a shot noise component. The last source of shot noise is due to the current flowing through the collector junction, I_{cob}.

Thermal noise is generated in the base, collector and emitter resistances. As both the collector and the emitter resistance are far smaller than the base resistance, the former two can be neglected. Although the base resistance is not lumped, but distributed, it can be approximated by one resistance. Therefore thermal noise can be modelled as originating form one resistor in the base.

The third type of noise, 1/f noise, is found in the base current and arises from statistical fluctuations in the conductivity of the semiconductor.

Summarising the above text, the noise sources are:

$$\overline{v_b^2} = 4\,k\,T\,R_b\,\Delta f$$

$$\overline{i_b^2} = 2\,q\,I_b\,\Delta f$$

$$\overline{i_{bf}^2} = 2\,q\,I_b\,\Delta f\,(f_1/f)$$

$$\overline{i_c^2} = 2\,q\,I_c\,\Delta f = 2\,k\,T\,g_f\,\Delta f$$

$$\overline{i_{co}^2} = 2\,q\,I_{cob}\Delta f$$

3.3 Modelling the noise sources

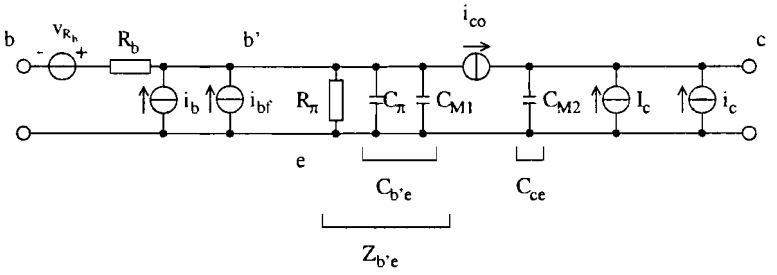

Figure 11: Hybrid π model with noise sources

Figure 11 shows the hybrid π model with the noise sources[6]. As for bipolar transistors the collector junction current, I_{cob}, is very small, the noise due to this current, i_{co}, can be neglected.

To obtain a model with one noise voltage and one noise current source, the noise sources can be referred to the input. A useful aid in this process are the parameters of the so called transmission matrix:

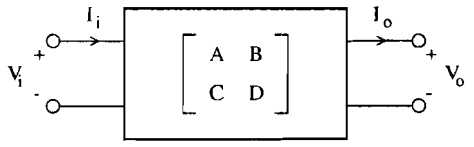

Figure 12: The transmission matrix

$$\begin{aligned} V_i &= A\,V_o + B\,I_o \\ I_i &= C\,V_o + D\,I_o \end{aligned} \tag{31}$$

The parameters A, B, C and D are defined as:

$$A = \left.\frac{V_i}{V_o}\right|_{I_o=0}, B = \left.\frac{V_i}{I_o}\right|_{V_o=0}, C = \left.\frac{I_i}{V_o}\right|_{I_o=0}, D = \left.\frac{I_i}{I_o}\right|_{V_o=0}. \tag{32}$$

Using the general π model of figure 13, the parameters can be calculated.

$$\begin{aligned} A &= \frac{Z_i}{g_f\,Z_{b'e}\,Z_o} & C &= \frac{1}{g_f\,Z_{b'e}\,Z_o} \\ B &= \frac{Z_i}{g_f\,Z_{b'e}} & D &= \frac{1}{g_f\,Z_{b'e}} \end{aligned} \tag{33}$$

[6]Noise sources are denoted small, normal sources by capitals

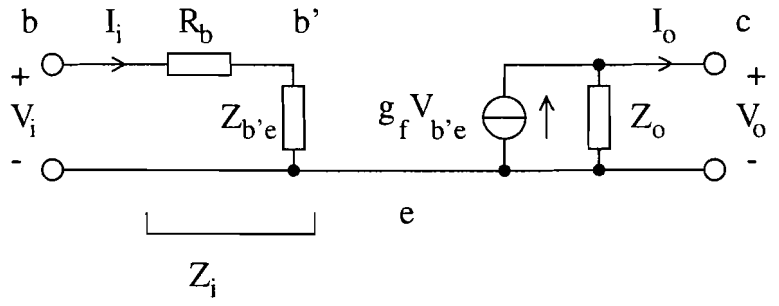

Figure 13: General π model for calculation of transmission parameters

3.4 Noise referred to the input of the open loop system

Using parameters B and D of the transmission matrix, the collector noise, i_c can be referred to the input resulting in a noise voltage source equal to $B\,i_c$ and a noise current source equal to $D\,i_c$. The two noise current sources from the internal base to ground, $i_b + i_{bf}$, can also be referred to an input noise voltage and current source. The current flowing from ground to the internal base can be substituted by a current flowing from ground to the external base, b, and a current flowing from the external base to the internal base, b'. The latter can also be represented as a voltage source in series with the base resistance, R_b. The transformation of these three noise sources is visualised in figure 14.

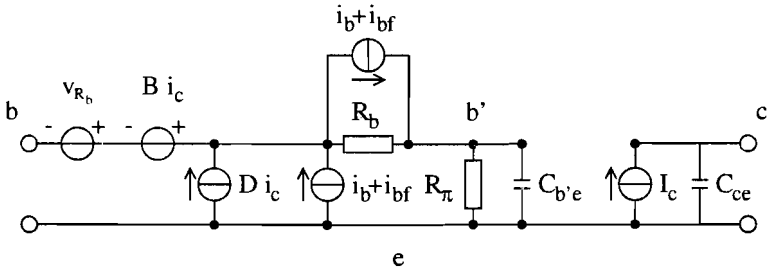

(a) All the noise sources referred to the input

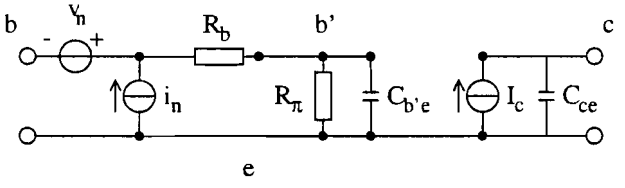

(b) To the input referred noise sources represented by one noise voltage source and one noise current source

Figure 14: Noise sources in the hybrid π transistor model

The resulting expressions for the input noise voltage source, v_n, and the input noise current source, i_n, are:

$$\begin{aligned} v_n &= v_{R_b} + B\, i_c + R_b\,(i_b + i_{bf}) \\ i_n &= D\, i_c + i_b + i_{bf} \end{aligned} \tag{34}$$

3.5 Noise referred to the input of the closed loop system

Similar to chapter one, the noise sources can be referred back to the input of the closed loop system. In this situation however, currents flow through the feedback loop. This has to be kept in mind when cutting open the feedback loop. Using the superposition theorem, the input noise voltage and current source of the open loop system can be referred back to the input of the closed loop system one by one. First, the noise voltage source will be referred back to the input of the oscillator.

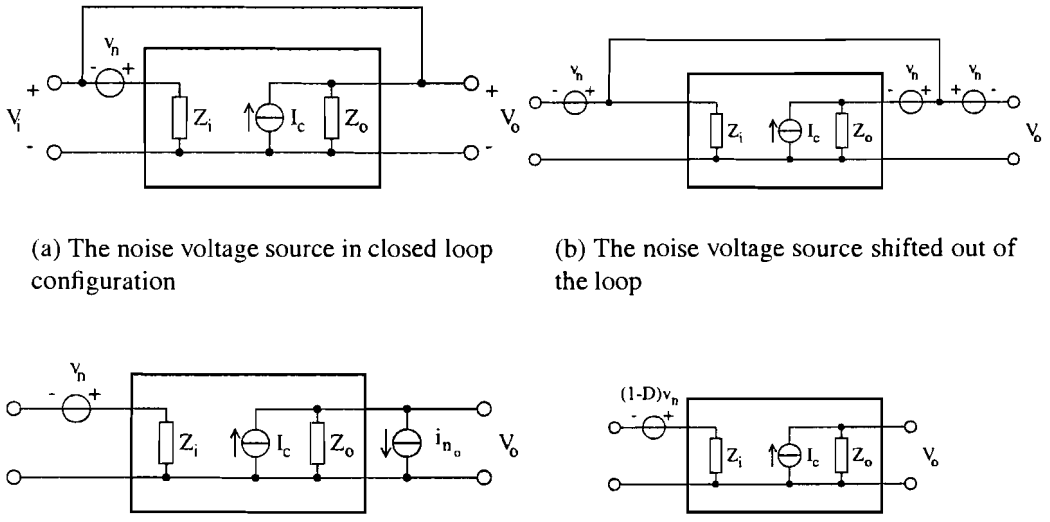

(a) The noise voltage source in closed loop configuration

(b) The noise voltage source shifted out of the loop

(c) The output voltage sources referred to one output current source

(d) All sources referred to one closed loop input source

Figure 15: Referring the open loop input noise voltage back to the input of the closed loop system

As a beginning, the noise voltage source is shifted out of the loop resulting in the sources as depicted in figure 15b. The two voltage sources at the output can be referred to one output current source, i_{n_o}. The voltage source in series with Z_o can be represented by a current source in parallel with Z_o. The voltage source in series with $Z_o//Z_i$ can be represented by a current source in series with $Z_o//Z_i$. As these sources are in parallel, they can be summed forming one output current source (figure 15c).

$$i_{n_o} = -\frac{v_n}{Z_o} + v_n \frac{Z_i\, Z_o}{Z_i + Z_o} = \frac{v_n}{Z_i} \tag{35}$$

At this stage, all currents through the feedback loop have been transformed to currents through other branches; the feedback loop can be cut open. Now the input noise voltage can be calculated by referring the output noise current to an input noise current (figure 15d). This input noise current can be multiplied by Z_i to obtain a voltage source that can be added to the voltage source already present at the input:

$$v_{i_v} = v_n - \frac{v_n}{Z_i} D Z_i = v_n (1 - D) \tag{36}$$

The same can be done for the open loop input noise current source. This process is depicted in figure 16. The current source can be referred to a closed loop input voltage source by recognising that the noise current can be seen as an output current resulting from an input voltage. Therefore the loop has to be cut open at point P. The input voltage needed to yield this output current is:

$$v_{i_i} = i_n B \tag{37}$$

As mentioned before, the two voltages, v_{i_v} and v_{i_i} can be summed to arrive at the total input noise voltage.

$$v_{nclp} = v_n (1 - D) + i_n B \tag{38}$$

Equation 38 will be used as the active circuit noise source in oscillators in the following chapter.

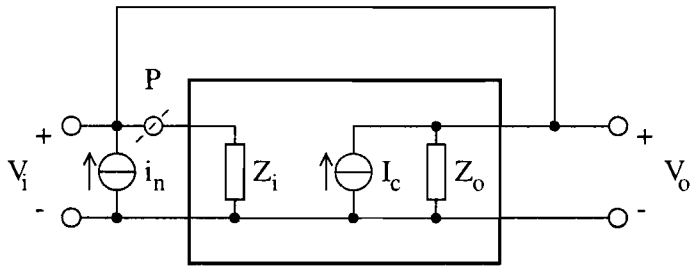

(a) The input current source in closed loop configuration

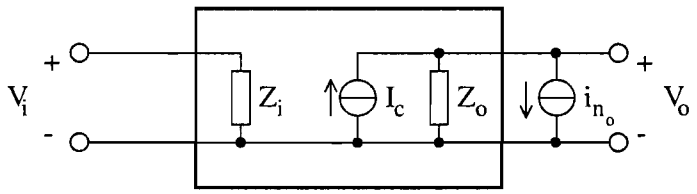

(b) The current source as output current

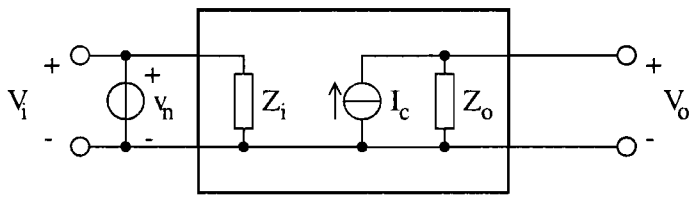

(c) The current source referred back to the input

Figure 16: Referring the open loop input noise current back to the input of the closed loop system

3.6 Conclusions

Noise due to the active part of the oscillator was examined in this chapter. The analysis was performed using a half circuit. Firstly, the noise sources were identified and referred back to the input of the open loop system. After that, the open loop input noise was referred to a closed loop input noise, resulting in equation 38. This expression will be used as the contribution of the active circuit to the total noise.

4 Noise in LC oscillators

In the previous chapters, expressions have been obtained for noise originating from both the resonator and the active circuit. The total output noise can be found by summing the two expressions for input noise and multiplying them by the closed loop transfer function. In section 4.1 the two input noise expressions are summed. Then, in section 4.2, the obtained input noise voltage is substituted in the approximate voltage noise equation to arrive at an approximate output noise voltage.

4.1 Combining passive and active circuit noise

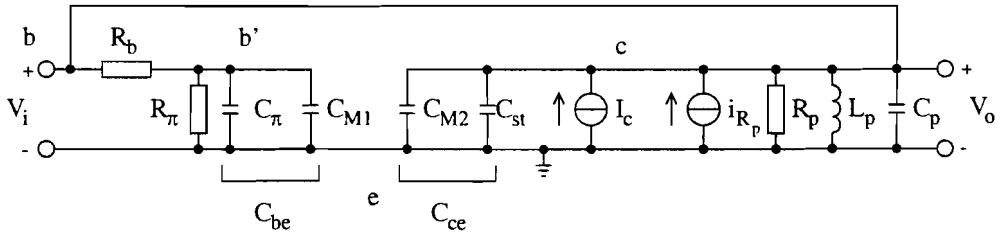

Figure 17: Resonator attached to π model

As figure 17 shows, the resonator is placed in parallel with the output impedance of the transistor. For an ac analysis this is valid; as all dc sources have a fixed value and the emitters of a differential amplifier are a virtual ground, the resonator can be regarded to be situated between the collector and the emitter. The noise generated by the LC resonator is represented by a noise current source between the collector and the emitter of the transistor, $i_{n_{R_p}}$, and equals the noise current of the frequency dependent resistor R_p:

$$i_{n_{R_p}}(j\omega) = \sqrt{\frac{4kT}{R_p(j\omega)}} \tag{39}$$

Comparing figure 17 to the hybrid π model from figure 11 it should be noted that two changes have been made. The output impedance has been changed:

$$Z_o = R_p//L_p//(C_p + C_{ce}) = \frac{j\omega R_p L_p}{R_p - \omega^2 L_p R_p (C_p + C_{ce}) + j\omega L_p} \tag{40}$$

and an extra noise current source, i_{R_p}, has been introduced parallel to I_c.

As i_c and i_{R_p} are in parallel, they can be summed. This leads to the following expression for the input noise (after equation 38)

$$\begin{aligned} v_{x_{clp}} &= v_n\,(1-D) + i_n\,B \\ &= (v_{R_b} + B\,(i_c + i_{R_p}) + R_b\,(i_b + i_{bf}))\cdot(1-D) \\ &\quad + (D\,(i_c + i_{R_p}) + (i_b + i_{bf})\,B \end{aligned} \tag{41}$$

Before multiplying this input noise voltage by the modulus of the closed loop transfer function, equation 41 has to be squared. Taking into account correlation this yields:

$$\begin{aligned} \overline{v_{x_{clp}}}^2 &= ((v_{R_b} + B\,(i_c + i_{R_p}) + R_b\,(i_b + i_{bf}))\,(1-D) + (D\,(i_c + i_{R_p}) + (i_b + i_{bf}))\,B) \\ &= (v_{R_b}\,(1-D) + (i_b + i_{bf})\,(R_B\,(1-D) + B) + (i_c + i_{R_p})\,(B\,(1-D) + B\,D \\ &= \overline{v_{R_b}}^2\,|1-D|^2 + \overline{(i_b + i_{bf})}^2\,|R_B\,(1-D) + B|^2 + \overline{(i_c + i_{R_p})}^2\,|B|^2 \end{aligned} \tag{4}$$

Equation 42 has been plotted versus simulation results[7]. The difference between the calculated mean squared noise voltage and the simulated mean squared noise voltage is within simulation accuracy.

4.2 Determining output noise using the approximate equation

Similar to chapter 2 an approximate expression for the output noise voltage can be found by using the Leeson-like equation. As in chapter 2, this equation,

$$\overline{v^2_{n_{Leeson-voltage}}(\omega)} = 4\,k\;T\;R_{l0}\frac{1}{{Q_{l0}}^2}\left(\frac{\omega_{osc}}{2\,\Delta\omega}\right)^2, \tag{43}$$

consists of a noise voltage source[8]: $4\,k\,T\,R_{lo}$ and a shaping function, $\frac{1}{Q_{lo}^2}\left(\frac{\omega_{osc}}{2\,\Delta\omega}\right)^2$, which is an approximation of the closed loop transfer function of the oscillator. As this approximate equation can be interpreted as a squared input noise voltage multiplied by an approximation of the closed loop transfer function, the squared input noise voltage from equation 42 can be substituted for the noise voltage source.

[7] The simulation file can be found in appendix D

[8] To describe the term involving the resistor as a noise source, a factor 4 has been introduced and is compensated for by the factor of 2 in $\frac{1}{Q_{lo}^2}\left(\frac{\omega_{osc}}{2\,\Delta\omega}\right)^2$

4.2.1 Deriving the oscillation frequency

To use the assumption in the Leeson-like approximate equation (i.e. $\omega \approx \omega_{osc}$) consistently, all frequency dependent terms in the input noise voltage are replaced by their values at ω_{osc}. As in chapter 2, ω_{osc} can be found by solving the Barkhausen criterion for ω.

$$\angle H(j\omega)_{openloop} = 0 \tag{44}$$

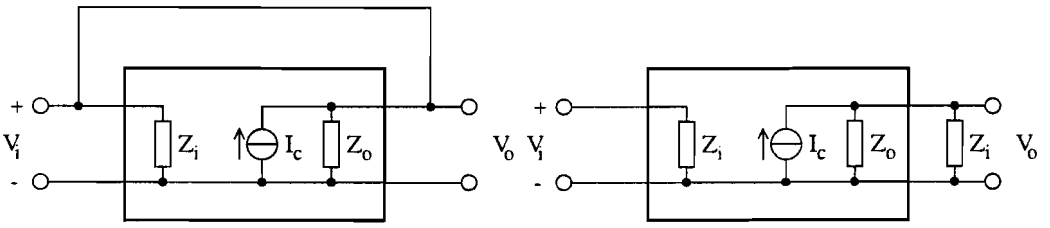

(a) Closed loop oscillator block with input and output impedances

(b) Open loop oscillator block with closed loop loading conditions

Figure 18: Loading in closed loop to open loop transformation

The open loop transfer function can be found by cutting open the feedback loop and adding the loading at the output as in figure 18. As $\frac{V_i}{V_u} = A$, the open loop transfer function is:

$$H(j\omega)_{openloop} = \frac{1}{A} = \frac{Z_i}{g_m Z_\pi Z_o} \tag{45}$$

Because of the loading Z_o has to be replaced by the parallel impedance of Z_i and Z_o: $\frac{Z_i Z_o}{Z_i + Z_o}$ yielding:

$$H(j\omega)_{openloop} = \frac{Z_i}{g_m Z_\pi \frac{Z_i Z_o}{Z_i + Z_o}} = \frac{Z_i + Z_o}{g_m Z_\pi Z_o} \tag{46}$$

Solving ω_{osc} from equations 44 and equation 46 is tedious and involves the use of mathematical software. Therefore merely the result is presented:

$$\omega_{osc} = \left(\frac{-\left(C_{be} L^2 R_{pi}\right) - C_{ce} L^2 (R_b + R_{pi}) - C L^2 (R_b + 2R_c + R_{pi}) + C^2 R_c (L R_c (R_b + R_{pi}) - Rl (C_{be} (R_c Rl + R_b (R_c + Rl)) R_{pi} + C_{ce} R_c Rl (R_b + R_{pi})))}{2C^2 L^2 (C_{be} (R_b + R_c) R_{pi} + C_{ce} R_c (R_b + R_{pi}))} + \frac{(-4(-(L (R_b + 2R_l + R_{pi})) + R_l (C_{be} (R_b + R_l) R_{pi} + C R_l (R_b + R_{pi}) + C_{ce} R_l (R_b + R_{pi})))}{2C^2 L^2 R_c (C_{be} (R_b + R_c) R_{pi} + C_{ce} R_c (R_b + R_{pi}))} \frac{\left(C L^2 (R_b + 2R_c + R_{pi}) + L^2 (C_{be} R_{pi} + C_{ce} (R_b + R_{pi})) + C^2 R_c (-(L R_c (R_b + R_{pi})) + Rl (C_{be} (R_c Rl + R_b (R_c + Rl)) R_{pi} + C_{ce} R_c Rl (R_b + R_{pi})))\right)^2}{2C^2 L^2 R_c (C_{be} (R_b + R_c) R_{pi} + C_{ce} R_c (R_b + R_{pi}))} \right)^{1/2} \right)^{1/2} \tag{47}$$

4.2.2 Deriving the resonator loaded quality factor, Q_l

Apart from the impedances due to the parallel resonator, the oscillator model of figure 17 shows several impedances that influence the quality factor of the resonator. To obtain an expression for the so called loaded quality factor, Q_l, the impedance in parallel with the collector current source can be transformed to a parallel circuit of a capacitor, an inductor and a resistor. To do so, the impedance network from base to emitter has to be transformed to a parallel capacitor, C_{eq}, and resistor, R_{eq}.

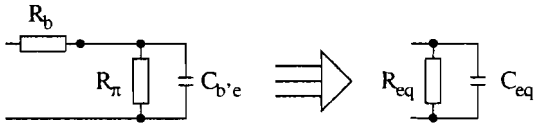

Figure 19: Transformation of network to parallel R and C

$$\begin{aligned} R_{eq} &= \frac{R_b{}^2 + 2\,R_b\,R_\pi + R_\pi{}^2 + C_{b'e}{}^2\,R_b{}^2\,R_\pi{}^2\,w^2}{R_b + R_\pi + C_{b'e}{}^2\,R_b\,R_\pi{}^2\,w^2} \\ C_{eq} &= \frac{C_{b'e}\,R_\pi{}^2}{2\,R_b\,R_\pi + R_\pi{}^2 + R_b{}^2\,\left(1 + C_{b'e}{}^2\,R_\pi{}^2\,w^2\right)} \end{aligned} \tag{48}$$

The parallel components R_p, L_p and C_p can now be expressed as:

$$\begin{aligned} R_t &= \frac{R_p\,R_{eq}}{R_p + R_{eq}} \\ &= \frac{Rp\,\left(R_b{}^2 + 2\,R_b\,R_\pi + R_\pi{}^2 + C_{b'e}{}^2\,R_b{}^2\,R_\pi{}^2\,w^2\right)}{\left(R_b + R_\pi + C_{b'e}{}^2\,R_b\,R_\pi{}^2\,w^2\right)\left(Rp + \frac{R_b{}^2 + 2\,R_b\,R_\pi + R_\pi{}^2 + C_{b'e}{}^2\,R_b{}^2\,R_\pi{}^2\,w^2}{R_b + R_\pi + C_{b'e}{}^2\,R_b\,R_\pi{}^2\,w^2}\right)} \\ &= \frac{Rp\,\left(2\,R_b\,R_\pi + R_\pi{}^2 + R_b{}^2\,\left(1 + C_{b'e}{}^2\,R_\pi{}^2\,w^2\right)\right)}{R_\pi\,\left(Rp + R_\pi\right) + R_b{}^2\,\left(1 + C_{b'e}{}^2\,R_\pi{}^2\,w^2\right) + R_b\,\left(Rp + 2\,R_\pi + C_{b'e}{}^2\,Rp\,R_\pi{}^2\,w^2\right)} \\ L_t &= L_p \\ C_t &= C_p + C_{ce} + C_{eq} \\ &= C_p + C_{ce} + \frac{C_{b'e}\,R_\pi{}^2}{2\,R_b\,R_\pi + R_\pi{}^2 + R_b{}^2\,\left(1 + C_{b'e}{}^2\,R_\pi{}^2\,w^2\right)} \end{aligned} \tag{49}$$

Similar to chapter 2 (eq. 21), the loaded quality factor can be expressed in terms of R_t, L_t and C_t.

$$Q_l = R_t\sqrt{\frac{C_t}{L_t}} \tag{50}$$

Equation 50 has to be made frequency independent for using it in the Leeson-like equation. Therefore, ω_{osc} is substituted, resulting in the loaded quality factor at ω_{osc}, Q_{lo}.

4.2.3 Approximate output noise of the π model oscillator with parallel resonator

Now ω_{osc}, Q_{lo} and the input noise voltage (equation 42) are known an expression for the output noise can be obtained that is equivalent to expression 23 from chapter 2. However, as opposed to equation 23, equation 51 takes into account the noisy active part of the oscillator as well. Above that a factor 2 has been introduced to account for the other half circuit in the differential pair oscillator[9].

$$\overline{v^2_{Leeson-voltage}(\omega)} = 2\,\overline{v_{x_{clp}}(\omega = \omega_{osc})}^2 \frac{1}{{Q_{l0}}^2} \left(\frac{\omega_{osc}}{2\,\Delta\omega}\right)^2 \tag{51}$$

4.3 Validity of the rule of thumb for total oscillator noise

In chapter 2.4 a rule of thumb was derived to determine the maximum frequency offset for which the error due to using the Leeson-like equation was still less than 1 dB. This rule of thumb was derived for an oscillator generating solely resonator noise. It would be convenient if this rule of thumb would still be applicable for a real oscillator, i.e. an oscillator generating both resonator noise and noise originating from the active part of the oscillator.

To show the usefulness of the Leeson-like equation applied to the whole oscillator, equation 51 can be compared to simulations. It is expected that the conditions for using the equation are quite similar to the conditions derived in chapter 2.

Figure 20a shows the simulated output noise, together with the approximated output noise. In figure 20b the difference between the two graphs is shown for several values of the resonator quality factor. From this picture it can be seen that the Leeson-like equation is indeed a reasonable approximation close to the carrier frequency and for the resonator quality factor, Q_{lo}, sufficiently high.

Table 2 lists the frequencies at which the error is $\pm$ 1 dB for several values of the resonator quality factor at ω_{osc}, Q_{l0}. The calculated values were estimated with the rule of thumb derived in chapter 2:

$$\Delta\omega_{max} = \left(1 - \frac{4.5}{Q^2_{l0}}\right) \cdot \frac{\omega_{osc}}{5.5} \tag{52}$$

It should be stressed that equation 52 is merely a rule of thumb to estimate the upper and lower frequency for which the Leeson-like equation is still a good approximation.

Table 2 shows that the measured values for the upper limit match the calculated value better than the measured value for the lower limit. This, however, is not surprising when taking into account that the equation for the approximate maximum offset frequency (eq. 29 and eq. 52) was derived from the upper limit and not from the lower limit.

[9] As discussed in chapter 3 the calculations were performed on a half circuit

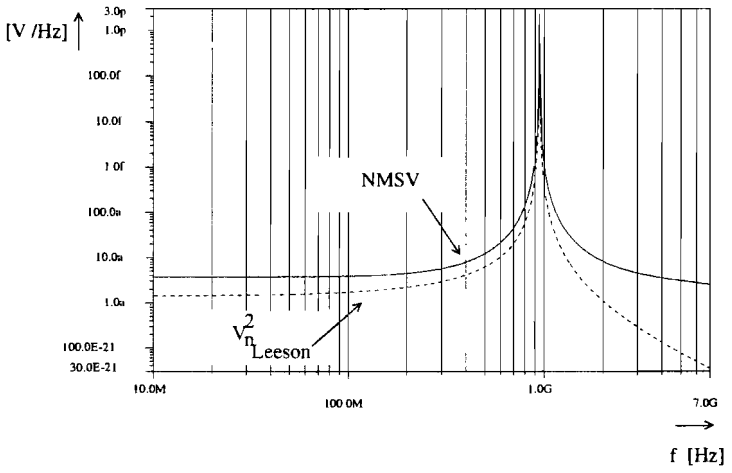

(a) Leeson's equation and simulated noise close to carrier

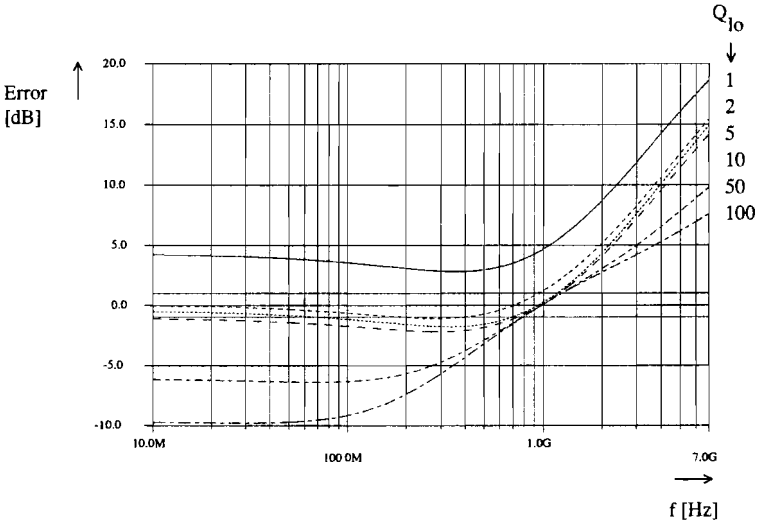

(b) Error due to using Leeson's equation as a function of the frequency

Figure 20: Approximate (Leeson-like) equation for the whole oscillator versus simulated noise

Q_{l0}	Calculated $\Delta\omega$ [MHz]	Measured $\Delta\omega$ [MHz]		Error @ ω_{osc} [dB]
		Down	Up	
1	-601	—	—	4.44
2	-22.2	584	—	1.11
3	89	374	120	0.49
4	129	321	170	0.27
5	147	293	192	0.18
10	172	251	224	0.06

Table 2: Applying the rule of thumb for several values of the loaded quality factor and f_{osc} = 1 GHz

4.4 Implementation loss

The approximate (Leeson-like) equations for the output noise voltage of the oscillator for the ideal situation (eq. 23 of chapter 2) and the situation with the noisy active part (eq. 51) give way to an interesting comparison. As the difference in noise is solely due to the transistors in the active part of the oscillator, it can now be established what the relative contribution of the noise, originating from the active part is, compared to the noise originating from the passive part. This **implementation loss**, that is a mathematical expression for the noise figure, F, of the amplifier is defined as:

$$L_{impl} = 10\,Log\left(\frac{N_{Passive+Active}}{N_{Passive}}\right) \tag{53}$$

in which N denotes the noise due to either both passive and active part or only active part.

A typical value for the implementation loss can be calculated using equations 51 and equation 23 from chapter 2. Taking the oscillation frequency to be 5 GHz, inductor and capacitor quality factors of respectively 16 and 35 at 2 GHz, and a tail current of 125 μA, the implementation loss is about 4 dB. So in this case, implementing the oscillator results in an increase of the voltage noise of 4 dB. One could also use this comparison to see what happens if, for example, I/Q functionality is implemented.

4.5 Conclusions

In this chapter the noise due to the active part of the oscillator circuit has been added to the noise due to the passive part of the oscillator. Again the Leeson-like equation has been derived by approximating the frequency dependent parameters by their value at ω_{osc}. It has been shown that the rule of thumb can still be applied.

Using the Leeson-like equation for both resonator noise and total noise, a new parameter, called implementation loss, has been defined. This parameter quantifies the increase in (phase) noise due to the active circuit; i.e. the increase in phase noise due to using a realistic transistor model instead of the ideal transconductance.

Implementation loss will later on be used to compare an LC oscillator to an I/Q LC oscillator.

5 Multi-Phase LC oscillators

In the previous chapters, single-phase LC oscillators were discussed, In this chapter the discussion will be expanded to multi-phase LC oscillators. It will be shown that due to coupling multiple LC oscillators, the expressions for the quality factor, and thus the CNR, show drastic changes.

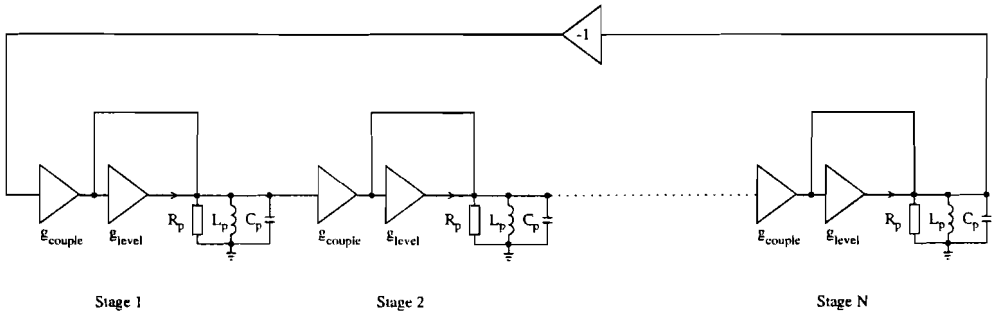

Figure 21: Behavioural model of N-stage LC oscillator

Figure 21 shows a common method to couple multiple LC oscillators to form an N-stage LC oscillator. When doing so the fact that the Barkhausen criterion has to be met, leads to drastic changes in the behaviour of the oscillator. Normally, an LC oscillator oscillates at a resonator phase shift close to zero degrees. When coupling N oscillators, every single oscillator is forced to oscillate at a frequency shift of $\frac{180°}{N}$. This can cause two problems. The first problem is that the oscillator does not oscillate with the maximum quality factor anymore, leading to a decrease in CNR. This problem is addressed in section 5.1. The second problem is, that the Barkhausen criterion can be met for multiple frequencies; a considerable risk of spurious oscillations is introduced, as shown in section 5.2.

5.1 The quality factor of a multi-phase LC oscillator

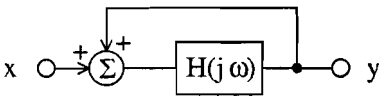

Figure 22: Oscillator model with open loop transfer function $H(j\,\omega)$

As Razavi [7] has shown, the quality factor of an LC oscillator can be calculated in terms of the transfer function of the oscillator:

$$Q = \frac{\omega_{osc}}{2}\sqrt{\left(\frac{\delta A}{\delta \omega}\right)^2 + \left(\frac{\delta \phi}{\delta \omega}\right)^2} \tag{54}$$

with

$$A = |H(j\,\omega)| \qquad and \qquad \phi = \angle(H(j\,\omega)) \tag{55}$$

with $H(j\,\omega)$ the open loop transfer function of the system as shown in figure 22.

A normal LC oscillator oscillates at a resonator phase shift of zero degrees. At zero degrees, $\frac{\delta A}{\delta \omega} = 0$ and therefore the quality factor can be written as:

$$Q = \frac{\omega_{osc}}{2} \frac{\delta \phi}{\delta \omega} \tag{56}$$

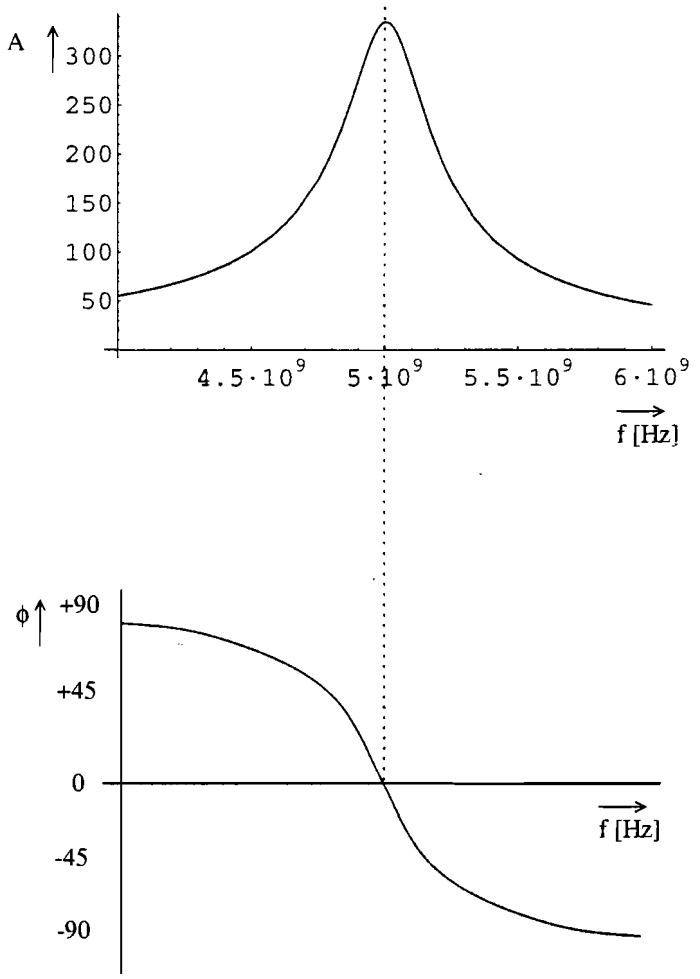

Figure 23: Modulus and argument of an LC resonator transfer function. The derivative of the phase shift (and thus the quality factor) is maximal at zero phase shift (marked by the dotted line)

Figure 23 shows that $\frac{\delta \phi}{\delta \omega}$ is maximum for a phase shift of zero degrees. Therefore the best resonator quality factor, and thus the best CNR, are achieved for an oscillator oscillating at zero degrees phase shift. As the N-stage architecture, shown in figure 21 requires the oscillator stages to oscillate at a phase shift of $\frac{180}{N}$ degrees[10], the resonator quality

[10] In practice this is not true as there is a phase shift due to the active part of the oscillator

factor will be far from optimal. By using an extra phase shift network when coupling LC oscillators, the phase shift does not have to be introduced by the oscillator sections themselves, resulting in a higher resonator quality factor.

5.1.1 Upper limit for the CNR of a multi-phase LC oscillator

Van der Tang [8] has shown that an upper limit can be derived for the attainable quality factor and thus CNR. Appendix E shows that the maximum quality factor for an N-stage LC oscillator is reached when the resonator in each oscillator stage oscillates at a phase shift of zero degrees. This quality factor then equals:

$$Q_{N_{max}} = N \cdot Q_p \tag{57}$$

Although improving the quality factor also improves the CNR (by a factor of 10 $\log N$)[11], this is merely an apparent improvement; as the oscillator consists of N sections, the power dissipation also increases with a factor of N. Using the same amount of power in a normal LC oscillator would result in the same CNR. But although no improvement in the CNR is observed, compared to a single-phase LC oscillator, there is also no reduction in the CNR of the multi-phase LC oscillator when the oscillator stages are oscillating at zero degrees resonator phase shift.

5.1.2 The effective quality factor

Apart from the useful knowledge that maximum attainable CNR of a multi-phase LC oscillator is as described in the last section, it is possible to derive some other interesting insights from Razavi's definition of the resonator quality factor. As this definition (eq. 54) shows, both the magnitude and phase of the transfer function influence the resonator quality factor. In normal situations, in which the oscillator oscillates at a resonator phase shift of zero degrees, the oscillator oscillates at the peak of $|H(j\omega)|$ and thus the term $\frac{\delta A}{\delta \omega}$ equals zero. In multi-phase LC oscillators, however, the oscillator phase shift is not equal to zero. As a result, the oscillator does not oscillate at the peak of $|H(j\omega)|$, and $\frac{\delta A}{\delta \omega}$ gets a value unequal to zero. The quality factor of the resonator oscillating at a phase shift of α degrees will be called effective quality factor, Q_{eff}. To calculate this effective quality factor as a function of the resonator phase shift, α, $\frac{\delta A}{\delta \omega}$ and $\frac{\delta \phi}{\delta \omega}$ have to be calculated. For multi-phase LC oscillators A and ϕ are defined as:

$$A = |H_N(j\,\omega)| \qquad and \qquad \phi = \angle(H_N(j\,\omega)) \tag{58}$$

As $H_N(j\,\omega)$ is obtained from the open loop oscillator transfer function, $H(j\,\omega)$, this transfer function is first calculated. For the behavioural model of one stage of an N-stage LC oscillator as in figure 24, the open loop transfer function is:

[11] As the CNR is a function of Q^2, one could expect 20 log N. However, the noise is also increased by a factor N compensating the quadratic factor

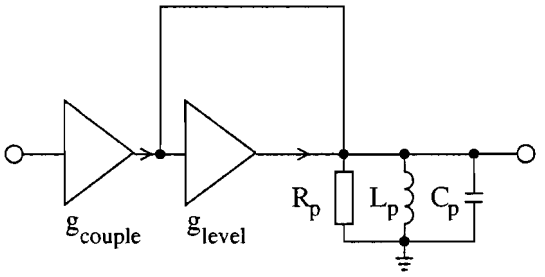

Figure 24: One stage of an N-stage I/Q LC oscillator

$$H(j\omega) = \frac{g_{couple}\, Z_p}{1 - g_{level}\, Z_p} \tag{59}$$

Substituting $Z_p = \frac{R_p}{1+j\,v\,Q_p}$ results in:

$$H(j\omega) = \frac{g_{couple}\, R_p\, \omega\, \omega_0}{\left(1 - g_{level}\, R_p\right) \omega\, \omega_0 + j\, Q_p\, \left(\omega^2 - {\omega_0}^2\right)} \tag{60}$$

Again ω_0 is equal to $\frac{1}{\sqrt{L_p\, C_p}}$. From equation 60, $|H(j\omega)|$ can be calculated to be

$$|H(j\omega)| = \frac{g_{couple}\, R_p\, \omega\, \omega_0}{\sqrt{\left(1 - g_{level}\, R_p\right)^2 \omega^2\, {\omega_0}^2 + {Q_p}^2 \left(\omega^2 - {\omega_0}^2\right)^2}} \tag{61}$$

and $\angle H(j\omega)$ equals

$$\angle H(j\omega) = -\arctan\left(\frac{Q_p\, \left(\omega^2 - {\omega_0}^2\right)}{\left(1 - g_{level}\, R_p\right) \omega\, \omega_0}\right). \tag{62}$$

The transfer function of an N-stage oscillator can be expressed in terms of the transfer function of the single-stage oscillator transfer function, $H(j\,\omega)$:

$$|H_N(j\,\omega)| = |H(j\,\omega)|^N = \frac{\left(g_{couple}\, R_p\, \omega\, \omega_0\right)^N}{\left(\left(1 - g_{level}\, R_p\right)^2 \omega^2\, {\omega_0}^2 + {Q_p}^2 \left(\omega^2 - {\omega_0}^2\right)^2\right)^{\frac{N}{2}}} \tag{63}$$

$$\angle H_N(j\,\omega) = N \cdot \angle H(j\,\omega) = -N \cdot \arctan\left(\frac{Q_p\, \left(\omega^2 - {\omega_0}^2\right)}{\left(1 - g_{level}\, R_p\right) \omega\, \omega_0}\right) \tag{64}$$

The effective quality factor can now be calculated by taking the derivative from equation 63 and equation 64,

$$\frac{\delta A}{\delta \omega} = -\frac{N Q_p{}^2 \left(\omega^4 - \omega_0{}^4\right) \left(\frac{g_{couple}{}^2 R_p{}^2 \omega^2 \omega_0{}^2}{\left(-1+g_{level} R_p\right)^2 \omega^2 \omega_0{}^2 + Q_p{}^2 \left(\omega^2-\omega_0{}^2\right)^2}\right)^{\frac{N}{2}}}{\left(-1 + g_{level} R_p\right)^2 \omega^3 \omega_0{}^2 + Q_p{}^2 \omega \left(\omega^2 - \omega_0{}^2\right)^2} \tag{65}$$

$$\frac{\delta \phi}{\delta \omega} = \frac{N Q_p \left(-1 + g_{level} R_p\right) w_0 \left(w^2 + w_0{}^2\right)}{\left(-1 + g_{level} R_p\right)^2 w^2 w_0{}^2 + Q_p{}^2 \left(w^2 - w_0{}^2\right)^2} \tag{66}$$

and substituting them in equation 54. As Q_{eff} is only meaningful at the oscillation frequency, ω_{osc} has to be substituted for ω in equations 65 and 66. The oscillation frequency can be obtained by determining the frequency at which the oscillator oscillates at a phase shift α. This means the following equation has to be solved:

$$\angle H(j\omega) = -\arctan\left(\frac{Q_p \left(\omega^2 - \omega_0{}^2\right)}{\left(-1 + g_{level} R_p\right) \omega \omega_0}\right) = \alpha \tag{67}$$

Solving equation 67 results in:

$$\omega_{osc} = \frac{\left(-1 + g_{level} R_p\right) \omega_0 \tan(\alpha) + \sqrt{4 Q_p{}^2 \omega_0{}^2 + \left(-1 + g_{level} R_p\right)^2 \omega_0{}^2 \tan(\alpha)^2}}{2 Q_p} \tag{68}$$

To comply with the Barkhausen criterion the gain has to be equal to 1 for $\omega = \omega_{osc}$. Choosing g_{level}, g_{couple} has to be chosen such that:

$$|H(j\omega)| = \frac{g_{couple} R_p \omega \omega_0}{\sqrt{\left(-1 + g_{level} R_p\right)^2 \omega^2 \omega_0{}^2 + Q_p{}^2 \left(\omega^2 - \omega_0{}^2\right)^2}} = 1 \tag{69}$$

for $\omega = \omega_{osc}$. Substituting the found expression for ω_{osc} (eq. 68) for ω in equation 69 yields:

$$|H(j\omega)| = \frac{g_{couple} R_p \cos(\alpha)}{\left(-1 + g_{level} R_p\right)} \tag{70}$$

Now the identity $|H(j\omega)| = 1$ can be solved for g_{couple}, resulting in:

$$g_{couple} = \frac{-1 + g_{level} R_p}{R_p \cos(\alpha)} \tag{71}$$

Equation 71 shows that there are innumerable combinations of g_{level} and g_{couple} that fulfill the condition $|H(j\omega)| = 1$ and thus result in oscillation. For a noise analysis however, the value of g_{level} is restricted. This limitation of the model originates from the internal feedback loop. In noise calculations the physical resonator quality factor is needed. When

compensating the resonator parallel resistance with the internal feedback loop and g_{level}, the resonator parallel resistance is electronically decreased. Thus, looking at the oscillator section as a black box with input g_{couple} and the resonator voltage as the output, it seems that the less energy has to be put into the system in order to sustain oscillation. As the resonator quality factor is proportional to the dissipated amount of energy, it seems that the resonator quality factor is higher than the physical resonator quality factor and even equals infinity for $g_{level} = \frac{1}{R_p}$ (no energy has to be put into the system in order to sustain oscillation). This energy is however put into the system via g_{level} and therefore the physical resonator quality factor has not been changed.

Figure 25 shows the electronically obtained quality factor as a function of g_{level}.

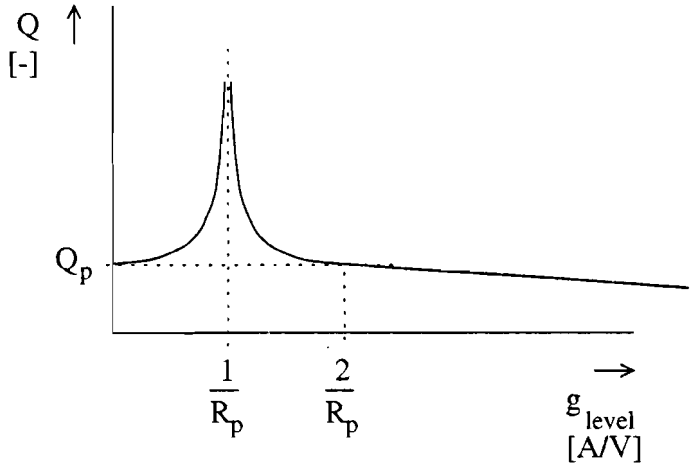

Figure 25: Electronically obtained quality factor as a function of g_{level}

As mentioned, for noise calculations, the physical resonator quality factor has to be used, and thus g_{level} has to be chosen such that transconductance g_{couple} 'sees' a resistance equal to R_p. This can be accomplished for two values of g_{level}. Of course g_{level} can be chosen zero so that it does not compensate the resistor in any way. Or g_{level} can be chosen $\frac{2}{R_p}$. In this case g_{couple} sees a negative resistance equal to $-R_p$. This negative resistance results in the same quality factor as the positive resistance R_p. As choosing g_{level} equal to zero results in a new behavioural model, g_{level} will be chosen $\frac{2}{R_p}$.

This more or less intuitive approach can be checked using an expression for the maximum attainable quality factor in multi-phase LC oscillators. As [8] shows the maximum quality factor for an N-stage LC oscillator is obtained with a resonator phase shift of zero degrees and equals [12]:

$$Q_{N_{max}} = N \cdot Q_p \tag{72}$$

This expression should also result from the expression for Q_{eff} when α is taken to be zero. Substituting $\alpha = 0$ in the expression for Q_{eff} results in:

[12]This is merely an apparent improvement; as the oscillator consists of N sections, the power dissipation also increases with a factor of N. Using the same amount of power in a normal LC oscillator would result in the same CNR

$$Q_{eff}(\alpha = 0) = \left| \frac{N \cdot Q_p}{-1 + g_{level} R_p} \right| \tag{73}$$

Equation 73 shows that indeed g_{level} has to be chosen either $\frac{2}{R_p}$ or zero to obtain a quality factor of $N \cdot Q_p$ for $\alpha = 0$. Again the solution $g_{level} = 0$ is omitted as to preserve the behavioural model.

The now obtained expression relates a decrease in resonator quality factor to a non zero resonator phase shift, α, and can be used to describe the decrease in CNR in multi-phase LC oscillators. To obtain numerical values for Q_{eff}, values have to be substituted for all parameters in the expression for the effective quality factor.

k	$1.38 \cdot 10^{-23}$	J/K
T	300	K
R_p	1260 ($Q_p = 20$)	Ω
	630 ($Q_p = 10$)	Ω
	315 ($Q_p = 5$)	Ω
L_p	2	nH
C_p	507	fF

Figure 26 shows a plot of the quality factor versus the frequency for a nominal quality factor (the quality factor of one section of the oscillator, oscillating at a phase shift of zero degrees) of 5, 10 and 20 and for N = 2. For $\alpha = 0°$ the quality factor indeed equals $N \cdot Q_p$ as predicted by Van der Tang [8]. Both calculated and simulated quality factor are shown. The calculated quality factor is the solid line. The simulated quality factor is denoted by the rectangular marks.

To show the effect of the amount of oscillator sections, N, on the effective quality factor, figure 27 is plotted. This figure shows the effective quality factor for a fixed value of the nominal quality factor ($Q_p = 20$) and for several values of N. Again Q_{eff} is maximum at $\alpha = 0$, attaining the value of $N \cdot Q_p$. For α increasing from 0° towards $\pm 90°$, the effective quality factor decreases as expected.

Figure 26 clearly shows that the resonator quality factor decreases for phase shifts other than zero degrees. Using Q_{eff} and Leeson's equation,

$$CNR = -10\,Log\left[\frac{k\,T}{2\,P}\frac{1}{Q^2}\left(\frac{\omega_{osc}}{\Delta\omega}\right)^2\right] \tag{74}$$

a new approximation of the CNR for an arbitrary phase shift can be defined:

$$CNR_\alpha = -10\,Log\left[\frac{k\,T}{2\,P}\frac{1}{Q_{eff}(\alpha)^2}\left(\frac{\omega_{osc}}{\Delta\omega}\right)^2\right] \tag{75}$$

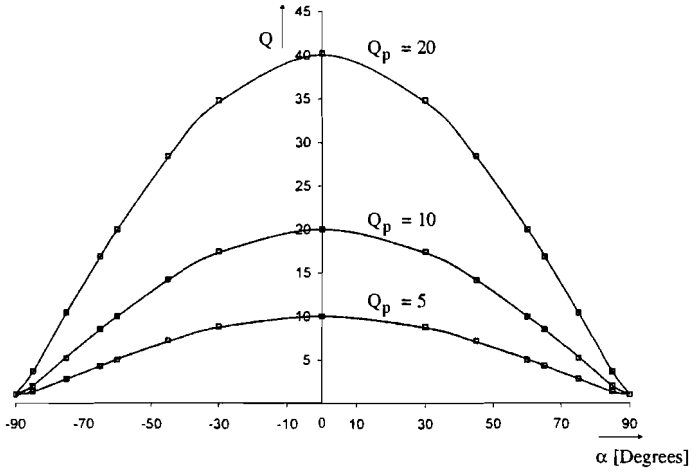

Figure 26: Plot of the effective quality factor, Q_{eff} versus the resonator phase shift, α for nominal quality factors of: Q_p = 5, 10, 20, f_{osc} = 5 GHz and N = 2

Similar to the effective quality factor, this equation can be plotted versus the resonator phase shift, α, as shown in figure 28.

As expected from the decrease in resonator quality factor with increasing resonator phase shift, the CNR also decreases with increasing resonator phase shift.

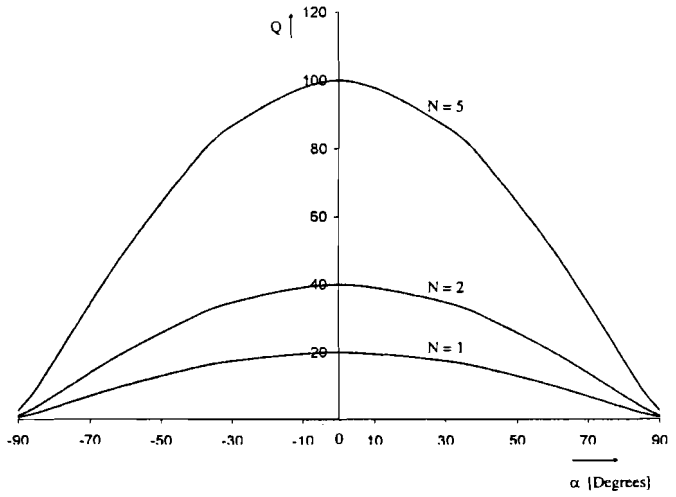

Figure 27: Plot of the effective quality factor, Q_{eff} versus the resonator phase shift, for N = 1, 2, 5, f_{osc} = 5 GHz and $Q_p = 20$

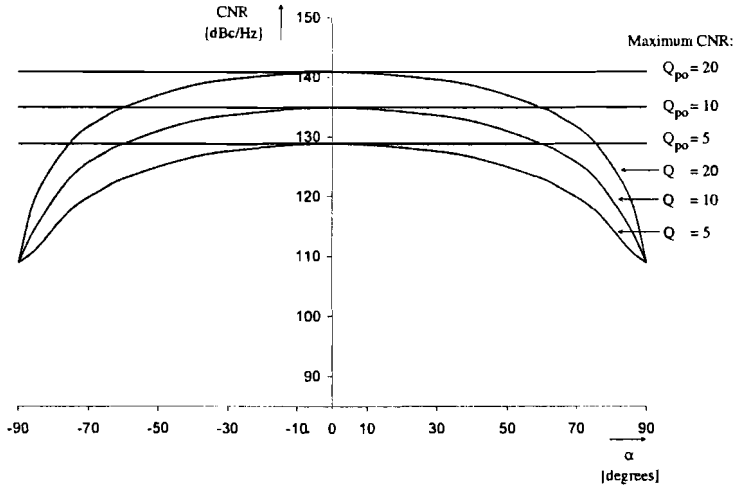

Figure 28: Plot of calculated CNR_α versus resonator phase shift, α for Q_p = 5, 10, 20 , f_{osc} = 5 GHZ and N = 2

5.2 Spurious oscillations

Apart from a decreasing CNR with increasing resonator phase shift, another problem arises for resonator phase shifts unequal to zero. To comply with the Barkhausen criterion an N-stage LC oscillator has to oscillate at a resonator phase shift of $\left|\frac{180°}{N}\right|$ degrees. This condition however, is fulfilled for two frequencies as can be seen in figure 29a. This figure shows an example for a four stage LC oscillator. If no explicit phase shift is applied, each section will oscillate at a resonator phase shift of $\frac{180°}{4} = 45°$. Both frequencies f_{-45} and f_{+45} fulfil this requirement. When applying a phase shift with the help of g_{couple}, of for example $-30°$, the resonator phase shift has either got to be $-15°$ (at f_{-15}) or $+75°$ (at f_{+75}). Figure 29b shows that the gain at frequency f_{-15} is higher than the gain at frequency f_{+75}. Therefore the oscillator will oscillate at frequency f_{-15}. However, due to non-linearities, in practical situations there is stil the risk of spurious oscillations. This risk is eliminated if the four stage oscillator is coupled with 45 degrees phaseshift.

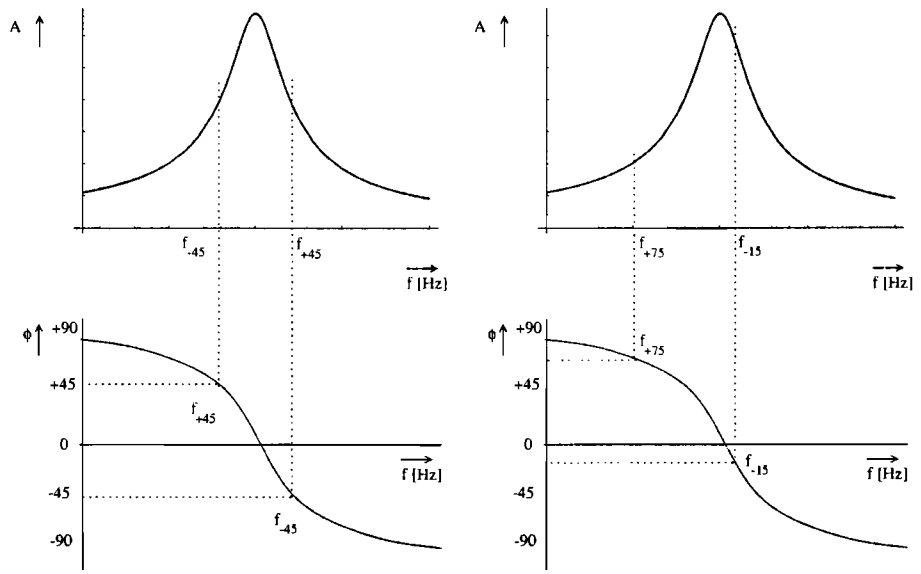

(a) Oscillation modes for zero explicit phase shift

(b) Oscillation modes for $-30°$ explicit phase shift

Figure 29: Oscillation modes for a four-stage LC oscillator with and without explicit phase shifts

5.3 Implementation loss of the 2-stage I/Q LC oscillator on a behavioural level

From figure 28 it is obvious that implementing multi-phase functionality will lead to a decrease in CNR, dependent on the resonator phase shift. As in chapter 4, section 4.4 an implementation loss can be defined. In this case the implementation loss is defined as:

$$\begin{aligned} L_{impl} &= 10\,Log\left(\frac{N_{Multi-phase}}{N_{single-phase}}\right) \equiv CNR_{single-phase} - CNR_{Multi-phase} \\ &= CNR_{single-phase} - CNR_{\phi} \end{aligned} \tag{76}$$

which represents the losses due to implementing the multi-phase functionality. As $CNR_{single-phase}$ is independent of the resonator phase shift (for single phase oscillators the phase shift is zero) and CNR_{ϕ} is known, the implementation loss can be determined. Theoretically for a resonator phase shift of zero degrees, the implementation loss will be zero. Figure 30 shows the CNR for all values of the resonator phase shift.

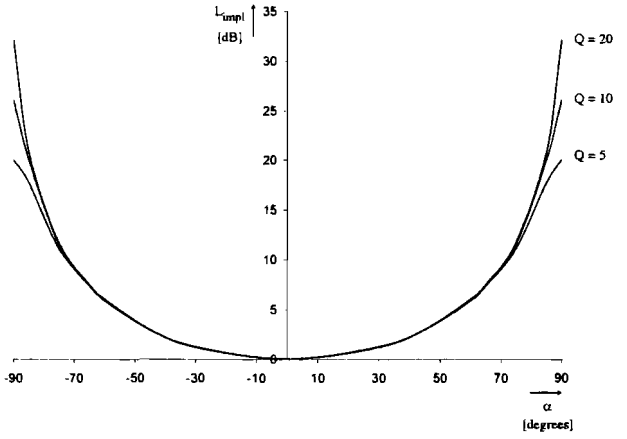

Figure 30: Plot of the calculated implementation loss versus resonator phase shift, ϕ for Q_p = 5, 10, 20, f_{osc} = 5 GHz and N = 2

5.4 Conclusions

In this chapter a theory was presented concerning the degradation of the CNR as a function of the resonator phase shift. The degradation of the quality factor as a function of the resonator has been checked. Although the degradation in CNR has not yet been checked it does satisfy the intuitive expectation that it decreases when the slope of the argument of the oscillator open loop transfer function decreases. Using CNR_ϕ the expected implementation loss can be determined. This implementation loss shows that it is possible to obtain multi-phase functionality without having to accept a decrease in CNR if the oscillator stages are coupled with an explicit phase shift of $\frac{180^\circ}{N}$. This explicit phase shift has another advantage: the risk of spurious oscillations is diminished.

6 Literature on I/Q LC oscillators

In section 5 it was found that special measures have to be taken in order to preserve a high resonator quality factor in multi-phase LC oscillators. A literature study on I/Q LC oscillators has been performed to gain insight on the present state of the art regarding this topic. An interesting question is whether existing architectures anticipate the reduction in resonator quality factor and what is being done to prevent this reduction. The study resulted in eight architectures, all of them based on two identical sections, each section containing a four transistor differential pair. These architectures are listed and briefly discussed in section 6.1. Then, in section 6.2, a selection is made from the found architectures. Finally conclusions are drawn in section 6.3.

6.1 State of the art architectures

In [9] an oscillator is presented consisting of two low-pass biquad filters as shown in figure 31. The differential pair used in the filters is different from the conventional differential pair as used in the LC oscillator from chapter 4. This results in a lower third-harmonic distortion component (a decrease by 20 dB) and a transconductance that is 64 % of the conventional differential amplifier. The in-phase and quadrature characteristics are obtained by connecting one filter stage to the other in phase and connecting the latter to the former 180° out of phase. This ensures that both oscillators have 90° phase shift in order to sustain oscillation.

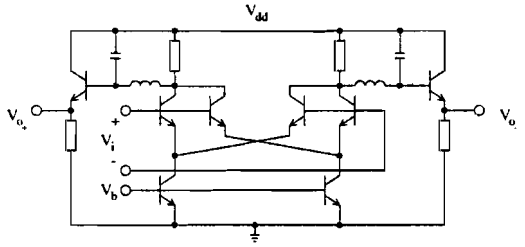

(a) Low-pass biquad filter

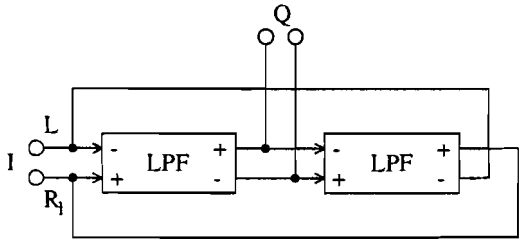

(b) Two low-pass biquad filters in ring configuration

Figure 31: I/Q LC oscillator based on two biquad low-pass filters

Figure 32 shows the topology proposed by Rofougaran c.s. [10]. Two conventional differential pair oscillators are used to obtain in-phase and quadrature signals. I/Q signals are generated in a fashion similar to [9].

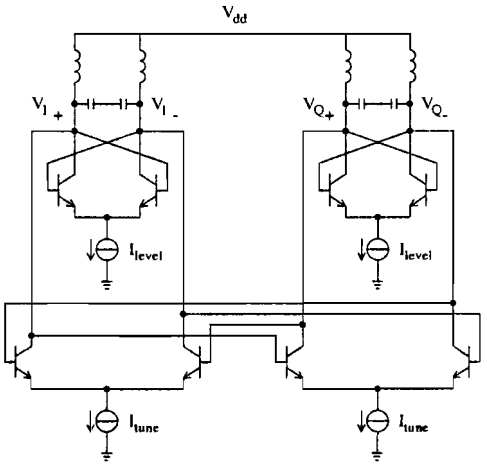

Figure 32: Two differential pair oscillators coupled in-phase and 180^o out of phase

Razavi [11] utilises the same architecture but at the same time introduces circuit techniques that increase the tuning range of the oscillator (see figure 33. By adding six transistors and two diodes the tuning range is increased by a factor of two.

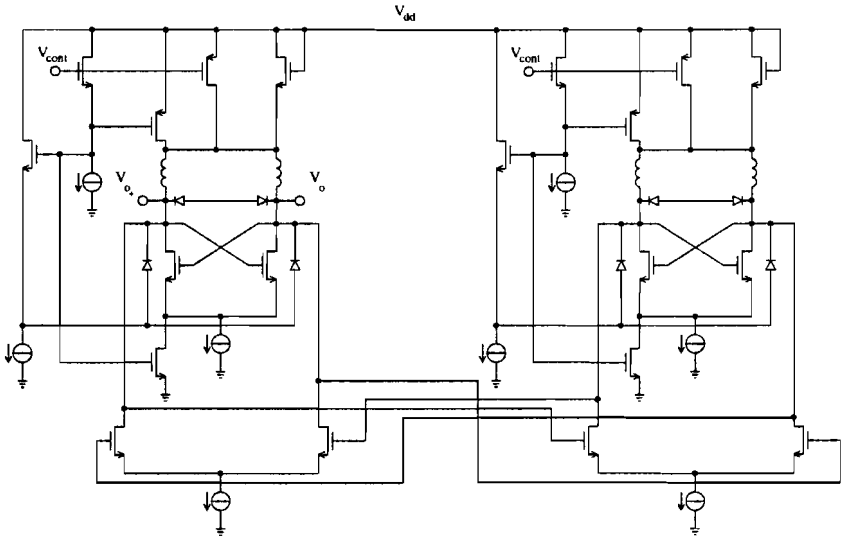

Figure 33: I/Q LC oscillator with increased tuning range

An oscillator consisting of the conventional differential pair, with buffered feedback and output (figure 34) is used in [12]. Along with improved inductor design techniques this decreases the phase noise at the cost of power dissipation.

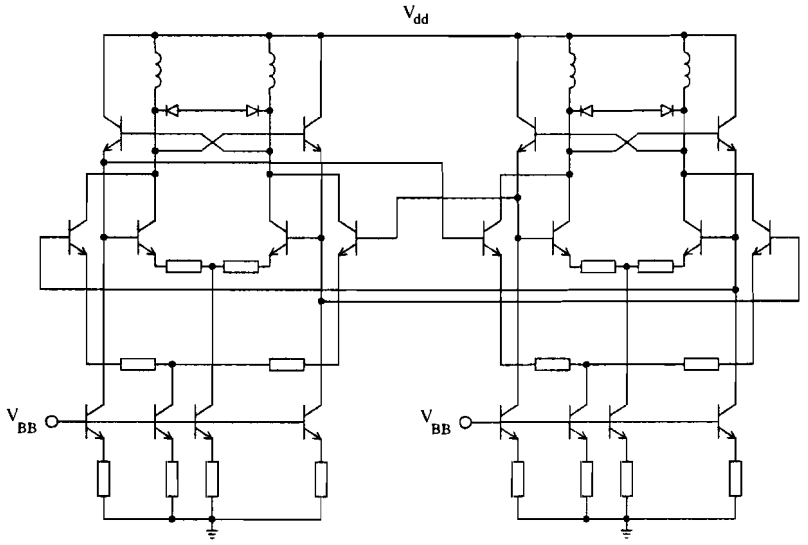

Figure 34: I/Q LC oscillator based on two differential pairs and buffering

A theory on reducing phase noise in the conventional differential pair oscillator by coupling the current sources is discussed in [13]. Apart from a reduction in the phase noise an improvement in amplitude and phase matching of about a factor of three is observed due to the named coupling of the current sources as depicted in figure 35 by the dashed line.

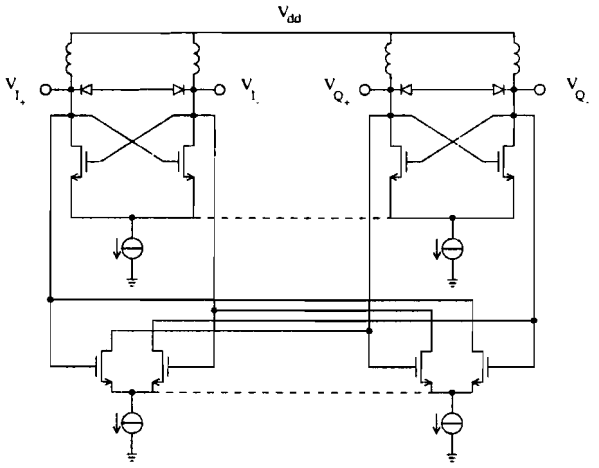

Figure 35: Reduction of phase noise by coupling the current sources

In [14] the effect of coupling more than two LC oscillator stages is discussed (see figure 48). Apart from the fact that more phases can be obtained, CNR increases with increasing number of stages. However, as discussed in chapter 7, coupling multiple stages also engenders an increase in power dissipation that exactly accounts for the increase in the CNR. Therefore the increase in CNR of an N-stage oscillator is equal to the CNR of a one stage LC oscillator oscillating with an output power of N times the power of each section of the N-stage oscillator.

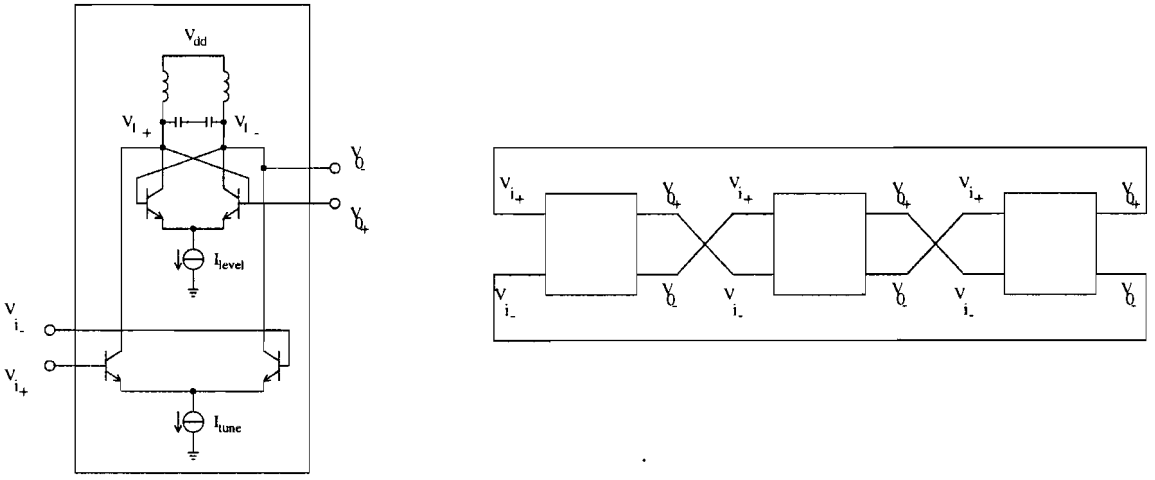

Figure 36: I/Q LC oscillator with more than two sections

Two very high frequency (10 GHz) oscillators, depicted in figure 37, are discussed in [15]. The first one is based on a ring-coupled quadrature oscillator. The second one is a four stage ring oscillator with an inductive load. Due to parasitics in the circuit the inductance behaves like an LC tank.

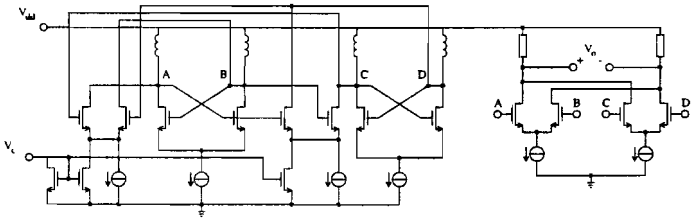

(a) Ring coupled quadrature VCO

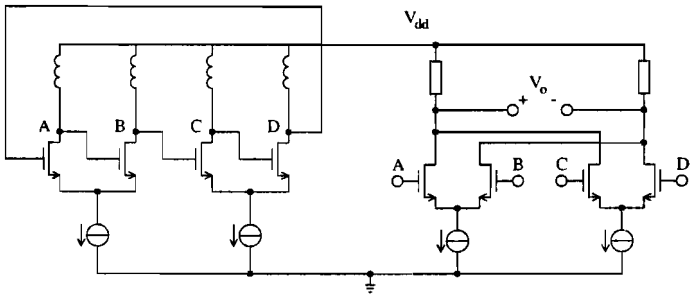

(b) Inductive load 4-stage ring oscillator

Figure 37: Very high frequency ring-coupled LC oscillators

Table 3 shows a list of the most important oscillator characteristics of the eight designs.

Literature number	f_{osc} [GHz]	Tuning Range [MHz]	Vdd [V]	Power dissi-pation [mW]	Technology	CNR [dBc/Hz]	CNR_{Norm} [dBc/Hz] [13]
[9]	1	227	5	50	0.8μm BiCMOS	-87 @ 100 kHz	-154
[10]	0.9	120	3	30	1μm CMOS Q_p = 5 @ 1GHz	-85 @ 100 kHz	-152
[11]	1.8	120	3.3	15.2	0.6μm CMOS	-100 @ 500 kHz	-162
[12]	1.9	120	2.7	86.4	Si Bipolar, f_τ = 40 GHz (SST-1C) Q_p = 8 @ 2 GHz	-123 @ 600 kHz	-177
[13]	0.9	100	2	44	MOSIS 0.8μm	-105 @ 100 kHz	-171
[14]	0.9	100	2.5	26	0.6μm, single-poly, triple-metal, CMOS	-132 @ 600 kHz	-181
[15] [14]	10.19	1240	1.5	45	0.25μm CMOS Q_p = 10 @ 12 GHz	-106 @ 1 MHz	-170
[15] [15]	12.38	400	1.5	24	0.25μm CMOS Q_p = 10 @ 12 GHz	-98 @ 1 MHz	-166

Table 3: Comparison of performance of the found topologies

[13] P_{ref} = 1mW

[14] Ring coupled quadrature oscillator

[15] Four stage ring oscillator with inductive load

6.2 Selection of architectures

Using one of the figures of merit (FOM) as described in [16], a selection[16] can be made from the found topologies. As a figure of merit not the TDE presented in [16] was taken, due to the fact that this FOM needs a value for the quality factor which is very often not presented in the papers. Therefore the following FOM was used:

$$CNR_{Norm} = -CNR_{design} + 10\,Log\left[\left(\frac{\Delta f}{f_{osc}}\right)^2 \frac{P_{DC}}{P_{ref}}\right] \tag{77}$$

For P_{ref} in equation 77 the value of 1 mW was chosen.

From CNR_{Norm} it should be concluded that both the architectures from [12] and [14] are promising. The oscillators proposed in [15] should not be omitted; although the CNR_{Norm} is somewhat lower than in the topologies of [12] and [14], the oscillators operate on a far higher frequency. Although the CNR_{Norm} also normalises for oscillation frequency, it does not take into account that it is harder to reach a certain quality value of the inductor at higher frequencies.

6.3 Conclusions

In this chapter various I/Q LC and other multi-phase oscillators were presented. The architectures were, more or less, compared to each other and a selection was made. Although a few promising architectures are presented, none of them keep in mind that the resonator quality factor is decreased by the coupling of multiple sections. Therefore it is expected that an architecture with phase shift networks will show a better CNR. Such an architecture is presented in the next chapter.

[16] Of course the other architectures may contain valuable ideas

7 An I/Q LC oscillator with explicit phase shift

The performed literature study has shown that many ways can be found to improve the CNR of I/Q LC oscillators. However, none of the articles take into account the problems that arise when coupling LC oscillators as described in chapter 5. In chapter 5, it was shown that the CNR deteriorates due to the way in which the oscillator stages are coupled and that there is a substantial risk of spurious oscillations. In this chapter an architecture is proposed [1] that eliminates the mentioned problems. In section 7.1 several phase shift networks are presented and their advantages and disadvantages are discussed. Then in section 7.2 one of the phase shifters is used in the proposed architecture [1]. Simulations are performed and results are presented in section 7.3. Finally in section 7.4, conclusions are drawn.

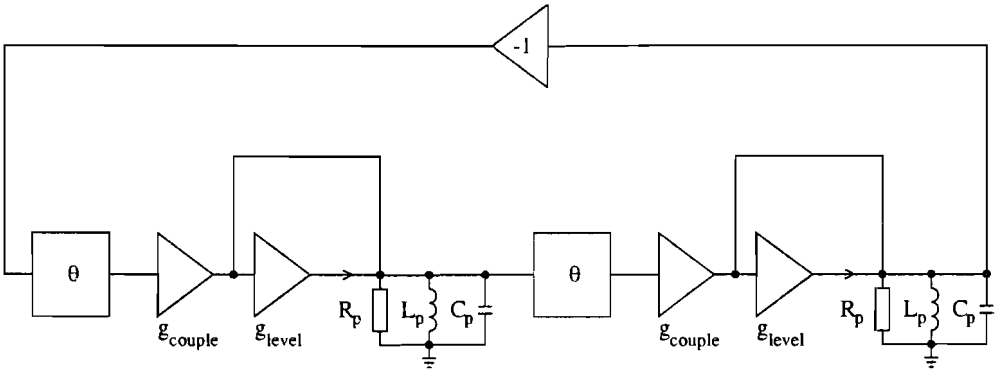

Figure 38: Behavioural model of the I/Q LC oscillator with explicit phase shift

7.1 Phase shift networks

From the theory described in chapter 5 it can be concluded that the best CNR will be obtained with an explicit phase shift, θ, of 90° minus the phase shift present due to the transistors. As a $\pm$ 90 degree phase shift for sinusoidal signals is the same as an integrating or differentiating action, it is possible to base the phase shift network on an integrator or a differentiator. For this design it was chosen to use a differentiator. Figure 39 shows several differentiator-like phase shifters.

Figure 39a shows a pure differentiator. The current I_{out} flowing into the collector shows a near -90 degree phase shift compared to the input voltage V_{in} for a certain frequency range. Using I_{diff}, this frequency range can be adjusted. This differentiator can be expanded with a buffering stage, resulting in figure 39b or a direct path (path without extra phase shift) resulting in 39c. Finally figure 39d shows a phase shifter that is not a differentiator, but also implements phase lead.

Using CNR and tuning range as criteria, the phase shifters from figure 39 were rated. With respect to the CNR it is expected that 39d performs best due to the absence of a noisy emitter current source. As 39a has one current source and both 39b and 39c two, it is expected that 39a shows a slightly better CNR. Phase shifter 39c however, offers

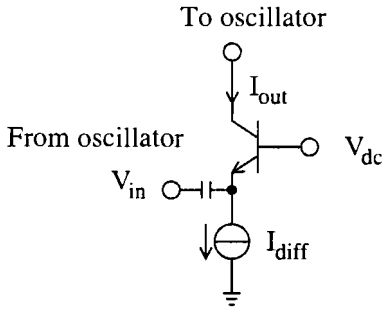

(a) Simple differentiator

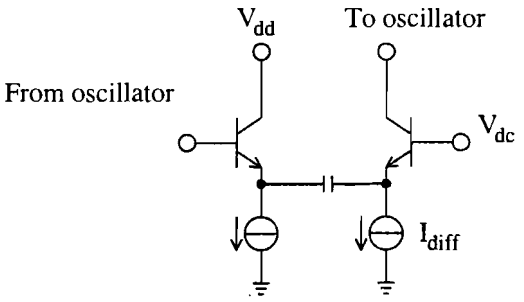

(b) Differentiator with buffering

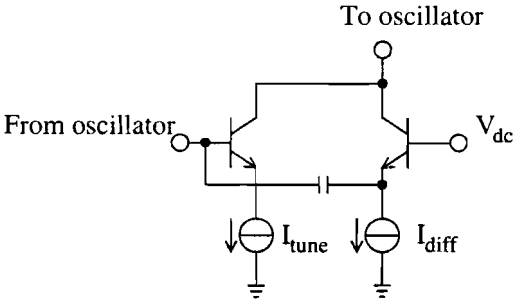

(c) Differentiator with tuning feature

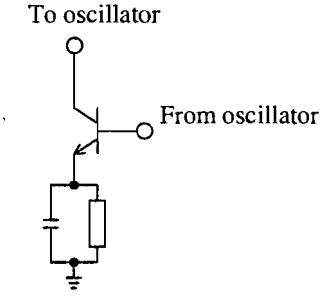

(d) Phase shifter with RC network

Figure 39: Several differentiator-like circuits

the possibility to tune the phase shift to exactly -90 degrees. Theoretically, if the tuning is performed properly, this phase shifter is expected to improve the CNR of the I/Q LC oscillator up to values observed in LC oscillators.

7.2 Implementation of the I/Q LC oscillator with explicit phase shift

Although at this stage of the project no choice has been made regarding the differentiators, the performance of the new architecture will be demonstrated using differentiator a from figure 39. Figure 40 shows the circuit diagram of the I/Q LC oscillator with phase shifters. Transistors Q1...Q14 are NPND transistors from the Cadence Qubic3 Library with an emitter area of 0.7 x 3.4 μm.

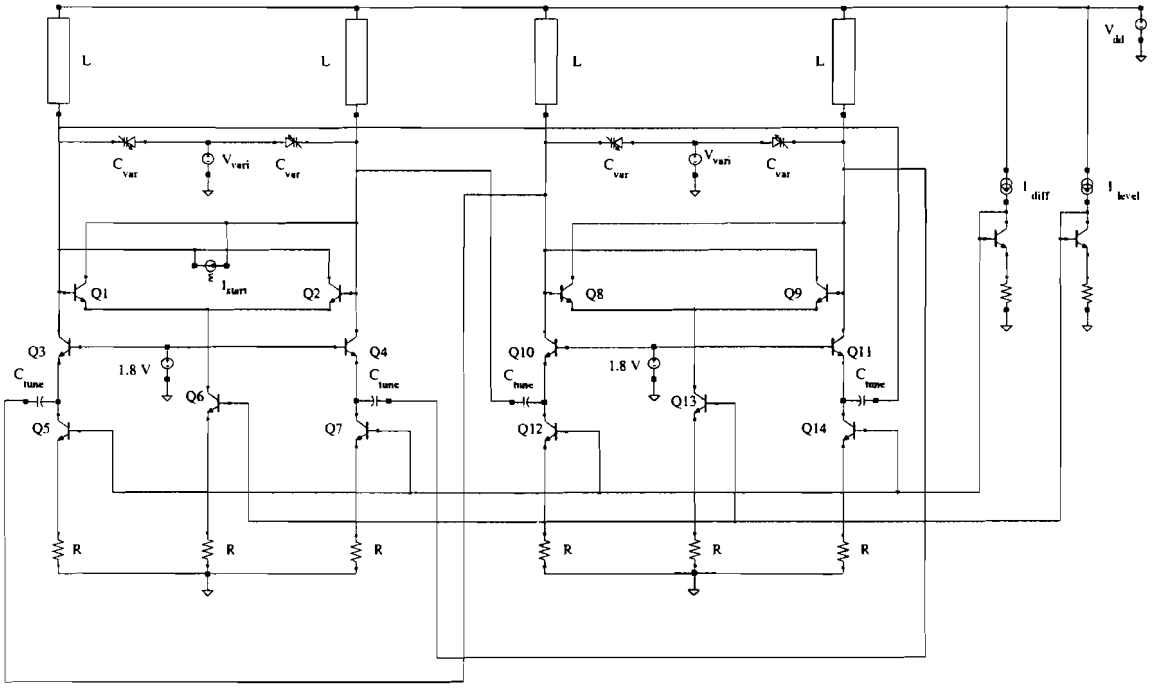

Figure 40: Circuit diagram of the I/Q LC oscillator with explicit phase shift

The two differential pair oscilator stages are formed with Q1 and Q2, respectivelly Q8 and Q9. The coupling between the two stages is performed by Q3, Q4, Q10 and Q11. Together with the resistors Q5 ... Q7 and Q12 ... Q14 form the necessary current sources. The resonator is made with the varactor diodes and the inductors, L. The model used for the inductors is shown in figure 41.

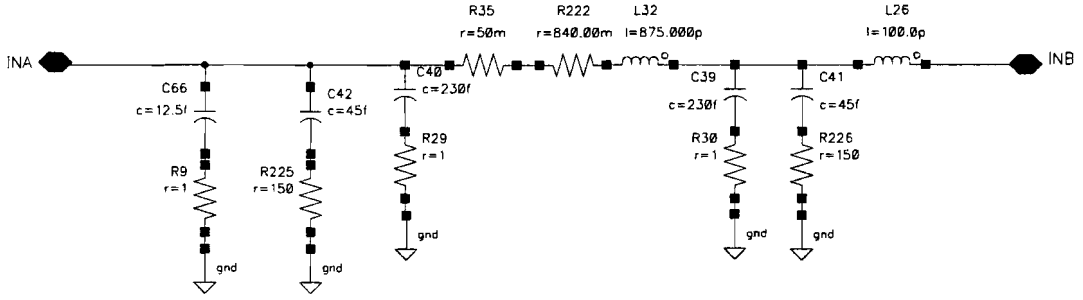

Figure 41: Model of the used inductor

7.3 Simulations and results

Due to time constraints the circuit from figure 40 has not yet been optimised. Nevertheless, the circuit was simulated in Spectre to obtain a value for the CNR. The obtained CNR was compared to the CNR observed in a comparable single phase LC oscillator and another very common I/Q LC oscillator [10].

	Single-phase LC oscillator	Multi-phase LC oscillator [1]		Multi-phase LC oscillator [10]
Vdd	3 V	3 V	3 V	3 V
I_{level}	1 mA	400 μA	1.2 mA	1.2 mA
I_{diff}	—	50 μA	150 μA	300 μA
V_{vari}	1.35 V	1.35 V	1.35 V	1.35 V
C_{tune}	—	100fF	100fF	—
C_{var}	950 fF	650 fF	750 fF	850 fF
f_{osc}	5 GHz	5 GHz	5 GHz	5 GHz
Δf	2 MHz	2 MHz	2 MHz	2 MHz
P_{DC}	3 mW	3 mW	9 mW	9 mW
V_swing	497 mV	199 mV	639 mV	166 mV
CNR	117.8 dBc/Hz	110.9 dBc/Hz	118.6 dBc/Hz	103.4 dBc/Hz

Table 4: Simulation results of a single-phase LC oscillator and two multi-phase LC oscillators with comparable conditions

The schematic diagrams of the single-phase LC oscillator and the common multi-phase LC oscillator [10] are depicted in appendix F. Table 4 shows simulations of the CNR in the three LC oscillators. Columns 2 through 5 show the CNRs of the three different architectures for an oscillation frequency of 5 GHz. The parameters of the I/Q LC oscillator with explicit phase shift have been chosen such that this oscillator can both be compared to the single-phase LC oscillator and to the other I/Q LC oscillator [10]. I.e. a simulation has been performed with the same DC power in the LC oscillator and the I/Q LC oscillator with explicit phase shift (3 mW). And a simulation has been performed with the same DC power in the I/Q LC oscillator with explicit phase shifts and the commonly used I/Q LC oscillator (9 mW). The architectures have been simulated using the same resonator. Column 3 shows that theoretically there is still room for improvement as, according to the theory from chapter 5, it should be possible to obtain a CNR equal to the CNR of the single-phase LC oscillator. But although there is still room for improvement, columns 4 and 5 show that, an increase of CNR of 15.2 dB is observed in [1] compared to [10].

7.4 Conclusions

In this chapter, a new I/Q LC oscillator architecture has been introduced. This I/Q LC oscillator with explicit phase shift has several advantages compared to the commonly used I/Q LC oscillator architecture [10]. First of all an increase in CNR is observed. Secondly, the risk of spurious oscillations has been decreased. Although the design has not yet been optimised, valuable information was obtained from simulations: compared to the commonly used I/Q LC oscillator architecture [10], an increase of the CNR of 15.2 dB was observed in the I/Q LC oscillator with explicit phase shift.

8 Conclusions and Outlook

8.1 Conclusions

State of the art I/Q LC architectures are based on coupled sections without explicit phase shifters. Similar to single-phase LC oscillators, voltage swing and resonator quality factor have great influence on the CNR of the oscillator. As a result of this insight, in chapter 5 it became clear that considerable improvements can be obtained by using explicit phase shift networks. An improvement in CNR of 15.2 dB was found in the proposed I/Q LC oscillator with explicit phase shift compared to a commonly used I/Q LC architecture [10].

From the derived theory it is also expected that spurious oscillations are prevented due to the explicit phase shifts.

8.2 Outlook

As it is the only architecture that anticipates for the decrease in CNR due to phase shifts in the oscillator, the I/Q LC oscillator with explicit phase shifts as presented in chapter 7, will be optimised, processed and characterised. As a phase shifter, circuit c from figure 39 will be used.

References

[1] van der Tang J.D., D. Kasperkovitz, and P.W.J. van de Ven, "Correct-by-construction quadrature lc oscillator with exact 90 degrees phase shift," Patent proposal, 2000.

[2] A. Hajimiri and T. Lee, *The design of low noise oscillators*, Kluwer Academic Publishers, 1999.

[3] D.B. Leeson, "A simple model of feedback oscillator noise spectrum," in *Proc. of IEEE*, 1966, pp. 329–330.

[4] W.P. Robins, *Phase Noise in Signal Sources*, IEE Telecommunicaton Series 9. Peter Peregrinus Ltd., 1982.

[5] H. Barkhausen, von, *Lehrbuch der Elektronen-Roehren, Band 3, Rueckkopplung*, Verlag S. Hrizel, 1935.

[6] P.R. Gray and R.G. Meyer, *Analysis and Design of Analog Intergrated Circuits*, John Wiley & Sons, Inc., 3 edition, 1993.

[7] B. Razavi, "A study of phase noise in cmos oscillators," *IEEE Journal of Solid-State Circuits*, vol. 31, no. 3, pp. 331–343, March 1996.

[8] J.D. van der Tang, "Cnr of n-stage lc ring oscillators," 2000.

[9] R. Duncan, K. Martin, and A. Sedra, "A 1 ghz quadrature sinusoidal oscillator," in *IEEE 1995 Custom Integrated Circuits Conference*, 1995, pp. 91–94.

[10] A. Rofougaran, J. Rael, M. Rofougaran, and A. Abidi, "A 900mhz cmos lc-oscillator with quadrature output," in *ESSCIRC*, 1996, pp. 392–393.

[11] B. Razavi, "A 1.8ghz cmos voltage-controlled oscillator," in *ESSCIRC*, 1997, pp. 388–389.

[12] T. Wakimoto and S. Konaka, "A 1.9-ghz si bipolar quadrature vco with fully-integrated lc tank," in *Symposium on VLSI Circuits Digest of Technical Papers*, 1998, pp. 30–31.

[13] L. Chi-wa and H.C. Luong, "2-v 900-mhz quadrature coupled lc oscillators with improved amplitude and phase matching," in *ISCAS '99*, 1999, vol. II, pp. II–585–II–588.

[14] J. J. Kim and B. Kim, "A low-phase-noise cmos lc oscillator with a ring structure," in *ISSCC*, 2000, pp. 430–431,475.

[15] T.P. Liu, "1.5 v 10-12.5 ghz integrated cmos oscillators," in *Symposium on VLSI Circuits Digest of Technical Papers*, 1999, pp. 55–56.

[16] J.D. van der Tang and D. Kasperkovitz, "Total design efficiency: A new figure of merit for oscillator benchmarking," in *ISCAS*, 2000, vol. II.

A Dependency of the oscillation frequency on resonator quality factors

As shown in chapter 2 the oscillation frequency is not equal to $\frac{1}{\sqrt{LC}}$, as assumed in most studies, but depends on the series resistances of the capacitor and the inductor.

$$\omega_{osc} = \frac{\sqrt{L - C\,Rl^2}}{\sqrt{C\,L}\sqrt{L - C\,Rc^2}} \tag{78}$$

Equation 78 can also be written in terms of the value of inductor and capacitor quality value, respectively Q_i and Q_c, at the oscillation frequency. Expressing ω_{osc} in terms of these quality factors at ω_{osc}, $Q_{i_{osc}}$ and $Q_{c_{osc}}$, enables a designer to calculate the oscillation frequency as a function of desired, i.e. possible, quality factors. To obtain the frequency independent expressions for the quality factors, ω_{osc} is substituted resulting in expressions for the quality factors at $\omega = \omega_{osc}$:

$$\begin{aligned} Q_{i_{osc}} &= \frac{\omega_{osc}\,L}{R_l} \\ Q_{c_{osc}} &= \frac{1}{\omega_{osc}\,C\,R_c} \end{aligned} \tag{79}$$

Substituting those expressions in 78 yields:

$$\omega_{osc} = \sqrt{\frac{1}{C\,L}}\sqrt{\frac{{Q_{i_{osc}}}^2 + {Q_{c_{osc}}}^2\,{Q_{i_{osc}}}^2}{{Q_{c_{osc}}}^2 + {Q_{c_{osc}}}^2\,{Q_{i_{osc}}}^2}} \tag{80}$$

Equation 80 can be normalized to a frequency of 1 Hz, by dividing the expression by $\sqrt{\frac{1}{LC}}$.

$$\omega_{osc_{norm}} = \sqrt{\frac{{Q_{i_{osc}}}^2 + {Q_{c_{osc}}}^2\,{Q_{i_{osc}}}^2}{{Q_{c_{osc}}}^2 + {Q_{c_{osc}}}^2\,{Q_{i_{osc}}}^2}} \tag{81}$$

Plotting equation 81 as a function of both quality factors, results in figure 42. This figure shows that for capacitor and inductor quality factors in the range[17] of 2 to 25, $\omega_{osc_{norm}}$ varies between 0.89 and 1.12. For $Q_{c_{osc}} = Q_{i_{osc}}$, ω_{osc} is precisely $\frac{1}{\sqrt{LC}}$.

[17] Quality factors less than 2 can result in a total quality factor less than 1; i.e. physically the resonator is no LC resonator anymore. Capacitor and inductor quality factors greater than 25 result in an oscillation frequency within 0.5 % around $\frac{1}{\sqrt{LC}}$

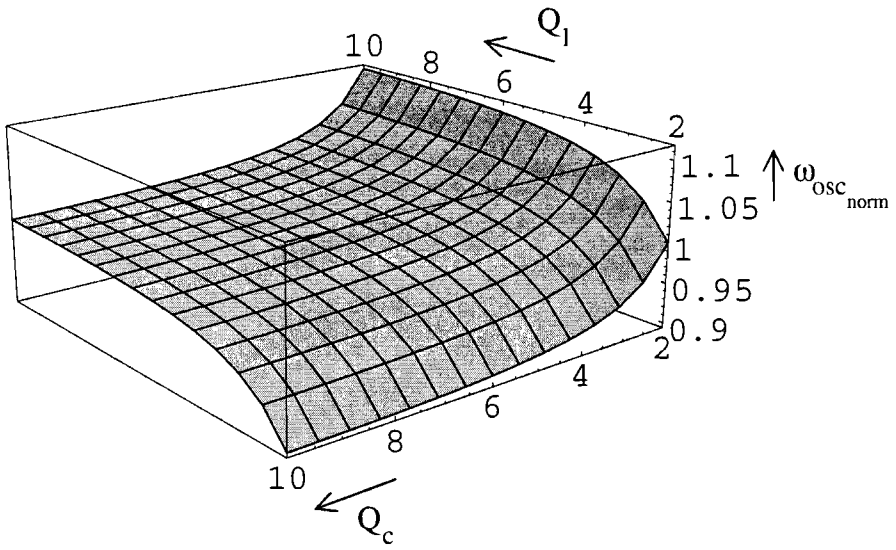

Figure 42: Normalised oscillation frequency as a function of Q_i and Q_c

B Simulation file of resonator noise

```
numform:8;
circuit;
r_d    (In,0) i=v/1e3;
c_1    (1,Out) Ccap;
R_Ccap  (1,0) Rc;
L_1    (2,Out) L;
R_11   (0,2) Rl;
j1     (0,out) i= Gm*vn(Out);
end;


ac;
init;
  nodc;
end;
noise: In,0,Out,0;
f=an(1e8, 1e10, 1000);
Ccap = 1e-12;
Rl = 3;
Rc = 0.5;
k = 1.38e-23;
Tk = 300;
Gm = (Ccap*(Rc + Rl))/(L + Ccap*Rc*Rl);
w = 2*pi*f;

w0 = 2*pi*1e9;
L =
(1+(w0*Ccap*Rc)**2+sqrt((1+(w0*Ccap*Rc)**2)**2-4*(w0*Ccap*Rl)**2))/
(2*Ccap*w0**2);
Dw = w-w0;

PhN1 = (4*k*Tk*((L + Ccap*Rc*Rl)**2)*
       (Rl + (Ccap**2)*(Rc**2)*Rl*(w**2)
     + (Ccap**2)*Rc*(Rl**2)*(w**2) +
       (Ccap**2)*(L**2)*Rc*(w**4)))/
       ((L - Ccap*(Rl**2) - Ccap*(L**2)*(w**2)
     + (Ccap**2)*L*(Rc**2)*(w**2))**2);

file: nmsv, PhN1,(nmsv-PhN1)/nmsv;
end;
run;

finish;
```

C Noise in an LC resonator with parallel resistance

Using the linear behavioural model of an LC oscillator shown in figure 43 an expression for the output noise voltage can be derived.

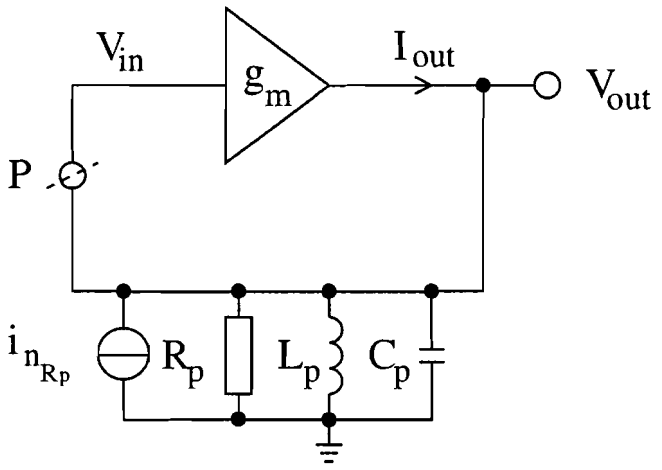

Figure 43: Simple model of an oscillator with noisy resonator

The impedance due to the parallel circuit of L_p, R_p and C_p can be written as:

$$Z_p(j\omega) = \frac{R_p}{1 + jvQ_p} \tag{82}$$

with

$$v = \frac{\omega}{\omega_0} - \frac{\omega_0}{\omega}$$

$$\omega_0 = \sqrt{\frac{1}{L_p C_p}} \tag{83}$$

$$Q_p = R_p\sqrt{\frac{C_p}{L_p}} = \frac{R_p}{\omega L_p} \tag{84}$$

and

$$|Z_p(j\omega)| = \frac{R_p}{\sqrt{1 + v^2 Q_p^2}} \tag{85}$$

$$\angle Z_p(j\omega) = \arctan(-vQ_p) \tag{86}$$

Cutting the feedback loop open at point P, the open loop transfer function can be obtained:

$$H(j\omega)|_{openloop} = \frac{V_{out}}{V_{in}}|_{openloop} = g_m Z_p \tag{87}$$

Now the closed loop transfer function can be calculated:

$$H(j\omega)\Big|_{\text{closed loop}} = \frac{V_{out}}{V_{in}}\Big|_{\text{closed loop}} = \frac{H(j\omega)|_{openloop}}{1 - H(j\omega)\Big|_{\text{open loop}}} = \frac{g_m Z_p(j\omega)}{1 - g_m Z_p(j\omega)} \tag{88}$$

Substituting equation 82 in equation 88 gives:

$$H(j\omega)\Big|_{\text{closed loop}} = \frac{V_{out}}{V_{in}}\Big|_{\text{closed loop}} = \frac{g_m R_p}{1 + j\, v\, Q_p - g_m R_p} \tag{89}$$

and

$$|H(j\omega)|\Big|_{\text{closed loop}} = |\frac{V_{out}}{V_{in}}|\Big|_{\text{closed loop}} = \frac{g_m R_p}{\sqrt{(1 - g_m R_p)^2 + (v\, Q_p)^2}} \tag{90}$$

The only noisy component in the oscillator model of figure 43 is the resistor, which produces a noise current equal to:

$$i_{n_R} = \sqrt{\frac{4\,k\,T\,B}{R_p}} \tag{91}$$

Assuming the feedback loop is cut open at point P this noise current can be transformed to the input by deviding the mean squared noise current by g_m^2. This results in:

$$\overline{v_{n_{in}}^2(\omega)} = \frac{4\,k\,T\,R_p}{(g_m R_p)^2} = \frac{4\,k\,T}{g_m^2 R_p} \tag{92}$$

In equation 92, B is taken to be 1 Hz, which physically means that the measurement bandwidth is assumed to be 1 Hz. Now the closed loop mean squared output noise voltage, $\overline{v_{n_{out}}^2(\omega)}$ can be obtained by multiplying $\overline{v_{n_{in}}^2(\omega)}$ by $|H(j\omega)|_{closedloop}$:

$$\begin{aligned}\overline{v_{n_{out}}^2(\omega)} &= \frac{4\,k\,T}{g_m^2 R_p}\frac{(g_m R_p)^2}{(1 - g_m R_p)^2 + (v\, Q_p)^2} \\ &= 4\,k\,T\,R_p\frac{1}{(1 - g_m R_p)^2 + (v\, Q_p)^2}\end{aligned} \tag{93}$$

D Simulation to verify the in chapter 4 found $v_{x_{clp}}$ (eq. 42)

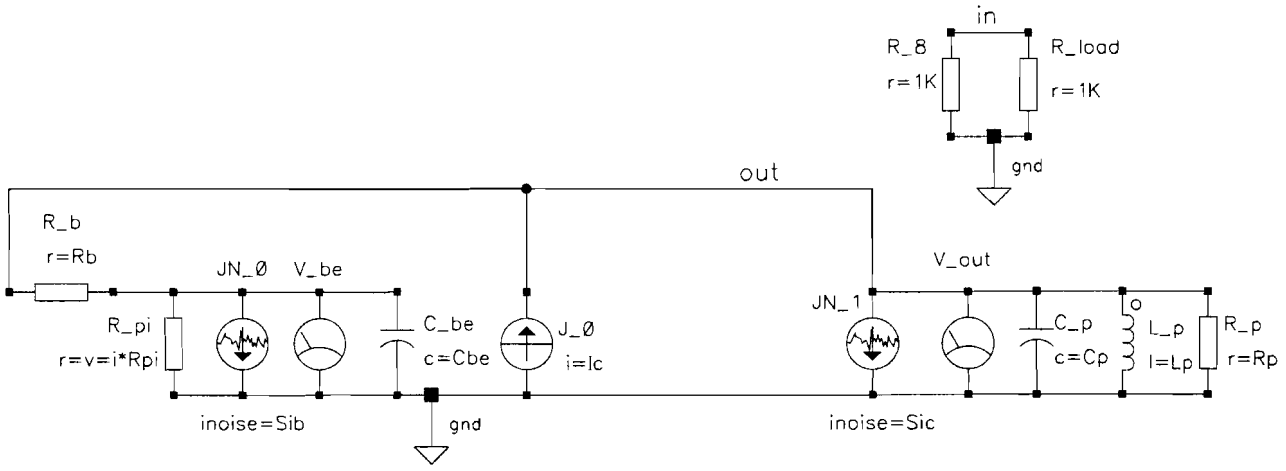

Figure 44: Schematics used for the simulation

Simulation file:

```
numform: 6;

ac;
init;
nodc;
end;

Temp=27;

RB    = 36.512;
RPI   = 23.806e03;
CB2   = 2.839E-15;
Cmu   = CB2;
CED   = 16.328e-15;
CET   = 7.176E-15;
Cpi   = CED+CET;
GF    = 3.697E-03;
Ic    = GF*V_be;
CST   = 7.790E-15;
CM1   = (1+Av)*Cmu;
CM2   = (1+1/Av)*Cmu;
CBE   = Cpi+CM1;
CCE   = CST+CM2;
Itail = 100u;
Beta = 132.6;

Av = 1;
Ib = Itail/(1+Beta);
Icn = Itail*Beta/(1+Beta);
q=1.6021918e-19;
```

```
k=1.3806226e-23;
T=300.15;

f=gn(1e6,10e9,200);
w = 2*pi*f;

Ri = 0.5;
Rc = 0.5;
Ccap = 1e-9/(4*pi**2);
L = 1e-9;
Ql = (w*L)/Ri;
Qc = 1/(w*Ccap*Rc);


Rp = ((Ri**2 + (L*w)**2)*(1 + (Ccap*Rc*w)**2))/
     (Ri + Ri*(Ccap*Rc*w)**2 + Rc*(Ccap*Ri*w)**2
   + Rc*(Ccap*L*(w**2))**2);
Cp = Ccap*Qc**2/(1+Qc**2);
Lp = L*(1+Ql**2)/Ql**2;


SvRb = 4*k*T*Rb;
SiRp = 4*k*T/Rp;
Sic = 2*q*Icn;
Sib = 2*q*Ib+2*q*Ib*(10/f);

SqrAbsHclosed =
(gf**2*Lp**2*Rp**2*Rpi**2*w**2)/
(Lp**2*Rpi**2*w**2 -
 2*Lp**2*Rp*Rpi*(-1 + gf*Rpi)*w**2 +
 Rb**2*(1 + Cbe**2*Rpi**2*w**2)*(Lp**2*w**2 +
 Rp**2*(-1 + Cp*Lp*w**2)**2) +
 2*Rb*(Lp**2*Rpi*w**2 + Rp**2*Rpi*(-1 + Cp*Lp*w**2)*
(-1 + Cp*Lp*w**2 + Cbe*gf*Lp*Rpi*w**2) +
 Lp**2*Rp*w**2*(1 - gf*Rpi + Cbe**2*Rpi**2*w**2)) +
 Rp**2*(Lp**2*w**2 - 2*gf*Lp**2*Rpi*w**2 +
 Rpi**2*(1 - 2*Cp*Lp*w**2 + gf**2*Lp**2*w**2 +
 Cbe**2*Lp**2*w**4 + Cp**2*Lp**2*w**4 + 2*Cbe*Lp*w**2*
(-1 + Cp*Lp*w**2))));

SqrAbsVxclp =
1/(gf**2*Rpi**2)*(Rb**2*(Sic + SiRp) + SvRb +
2*Rpi*(Rb*(Sic + SiRp) - gf*SvRb) +
Rpi**2*((1 + gf*Rb)**2*Sib + Sic + SiRp + gf**2*SvRb +
Cbe**2*Rb**2*Sic*w**2 + Cbe**2*Rb**2*SiRp*w**2 +
Cbe**2*SvRb*w**2));

MySout = SqrAbsVxclp*SqrAbsHclosed;

noise: in,0,out,0;
file: nmsv, MySout, 10*log(nmsv/MySout);
end;
run;
finish;
```

E CNR of N-stage LC ring oscillators

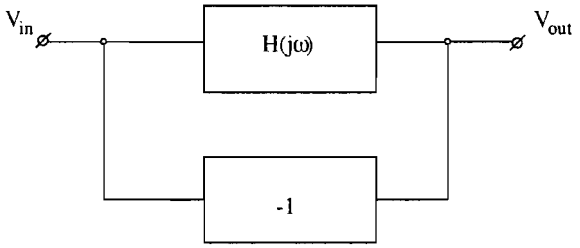

Figure 45: Oscillator feedback model.

Razavi [7] showed that if we treat an oscillator as a feedback system (such as shown in figure 45), the transfer function $|V_{out}/V_{in}|$ around the oscillation frequency can be approximated by:

$$\left|\frac{V_{out}}{V_{in}}(j(\omega_o + \Delta\omega))\right|^2 = \frac{1}{4Q^2}\left(\frac{\omega_o}{\Delta\omega}\right)^2 \tag{94}$$

In which Q is defined as:

$$Q = \frac{\omega_o}{2}\sqrt{\left(\frac{\delta A}{\delta\omega}\right)^2 + \left(\frac{\delta\phi}{\delta\omega}\right)^2} \tag{95}$$

and $A = |H(j\omega)|$ and $\phi = Arg(H(j\omega))$.

Now consider an N-stage LC oscillator illustrated in figure 46. Each LC oscillator stage is coupled by an all-pass filter which has unity gain for all frequencies and has a certain phase shift. For simplicity first a simple case is considered: the allpass filter has a fixed phase shift for all frequencies of π/N. N is the number of stages and is assumed to be at least 2.

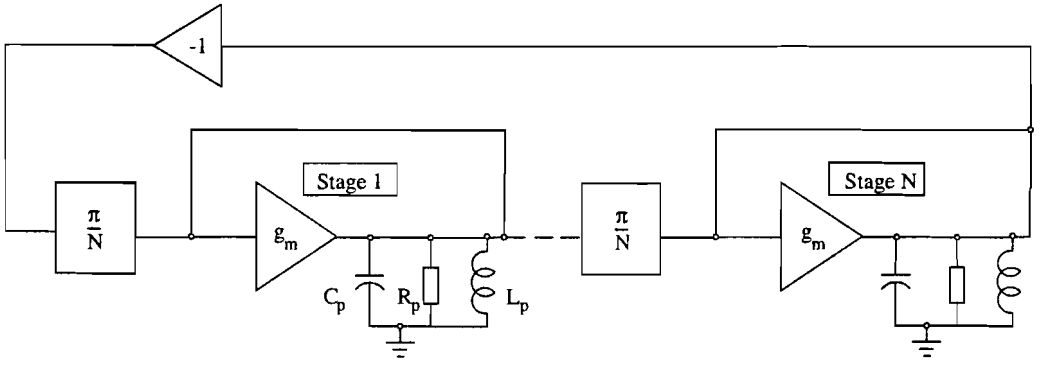

Figure 46: N-stage LC ring oscillator behavioural model.

For one stage the modulus of the transfer function is

$$|\frac{V_{out1}}{V_{in}}| = \frac{g_m R_p}{\sqrt{(1 - g_m Rp)^2 + (v Q_p)^2}} \tag{96}$$

with

$$v = \frac{\omega}{\omega_0} - \frac{\omega_0}{\omega} \tag{97}$$

$$Q_p = R_p \sqrt{\frac{C_p}{L_p}} = \frac{R_p}{\omega L_p} \tag{98}$$

$$\omega_0 = \frac{1}{\sqrt{L_p C_p}} \tag{99}$$

For an N-stage ring oscillator the modulus of the (open loop) transfer function is simply

$$|\frac{V_{outn}}{V_{in}}| = \frac{(g_m R_p)^N}{((1 - g_m Rp)^2 + (v Q_p)^2)^{\frac{N}{2}}} \tag{100}$$

And the argument $Arg(V_{outn}/V_{in})$ is N times the argument of a single stage:

$$Arg\left(\frac{V_{outn}}{V_{in}}\right) = -N\,(\frac{\pi}{N} + \arctan(vQ_p)\,) = -\pi - N\arctan(vQ_p) \tag{101}$$

In order to derive the quality factor of an N-stage LC oscillator $\delta A/\delta\omega$ and $\delta\phi/\delta\omega$ are calculated.

$$\frac{\delta A}{\delta\omega}\Big|_{\omega = \omega_0} = 0 \tag{102}$$

$$\frac{\delta\phi}{\delta\omega}\Big|_{\omega = \omega_0} = \frac{2 * N * Q_p}{w_0} \tag{103}$$

Therefore the Quality factor of an N-stage LC oscillator can be calculated using equation 95. This quality factor is valid under the condition that each LC-stage is coupled with π/N phase shift.

$$Q_{lcring} = N * Q_p \tag{104}$$

Using equation 94, removing AM and applying the oscillation condition $g_m = R_p$, the CNR for an N-stage LC oscillator can be formulated.

$$CNR(fm) = -10\log\left(\frac{NkT}{2P}\,\frac{1}{(N * Q_p)^2}\left(\frac{f_0}{f_m}\right)^2\right) \tag{105}$$

Notice that the original noise source kT of a single phase oscillator is now NkT since there are N noise sources. Since the only noise source is (N times) R_p, equation 105 can be considered a theoretical limit.

F Circuit diagrams used for simulations

Figures 47 and 48 respectively show the I/Q LC oscillator [10] and the single phase LC oscillator as used in the comparison of chapter 7.

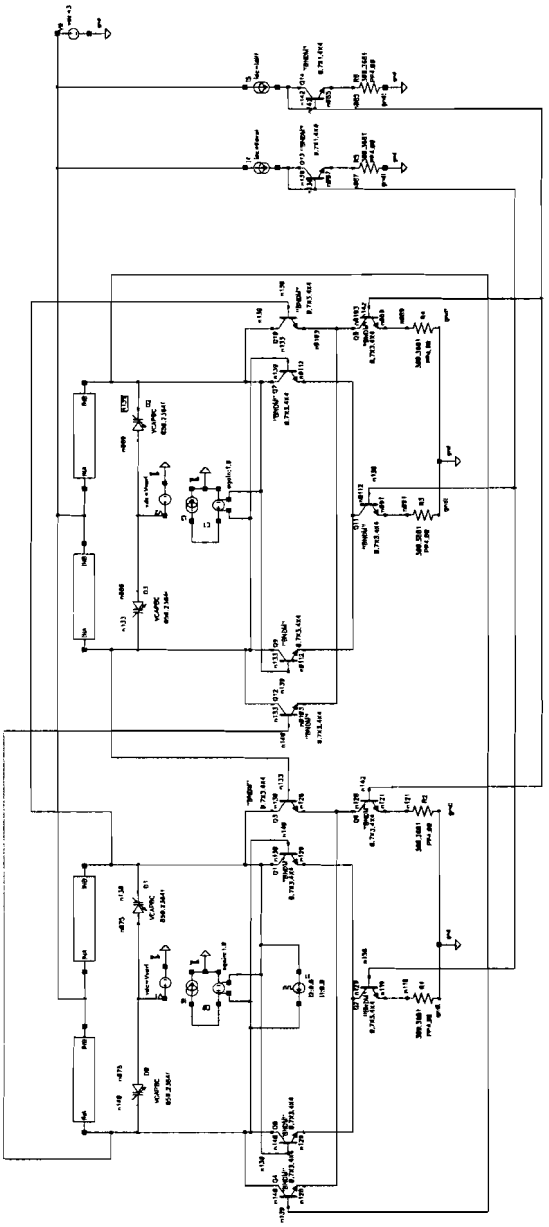

Figure 47: I/Q LC oscillator [10]

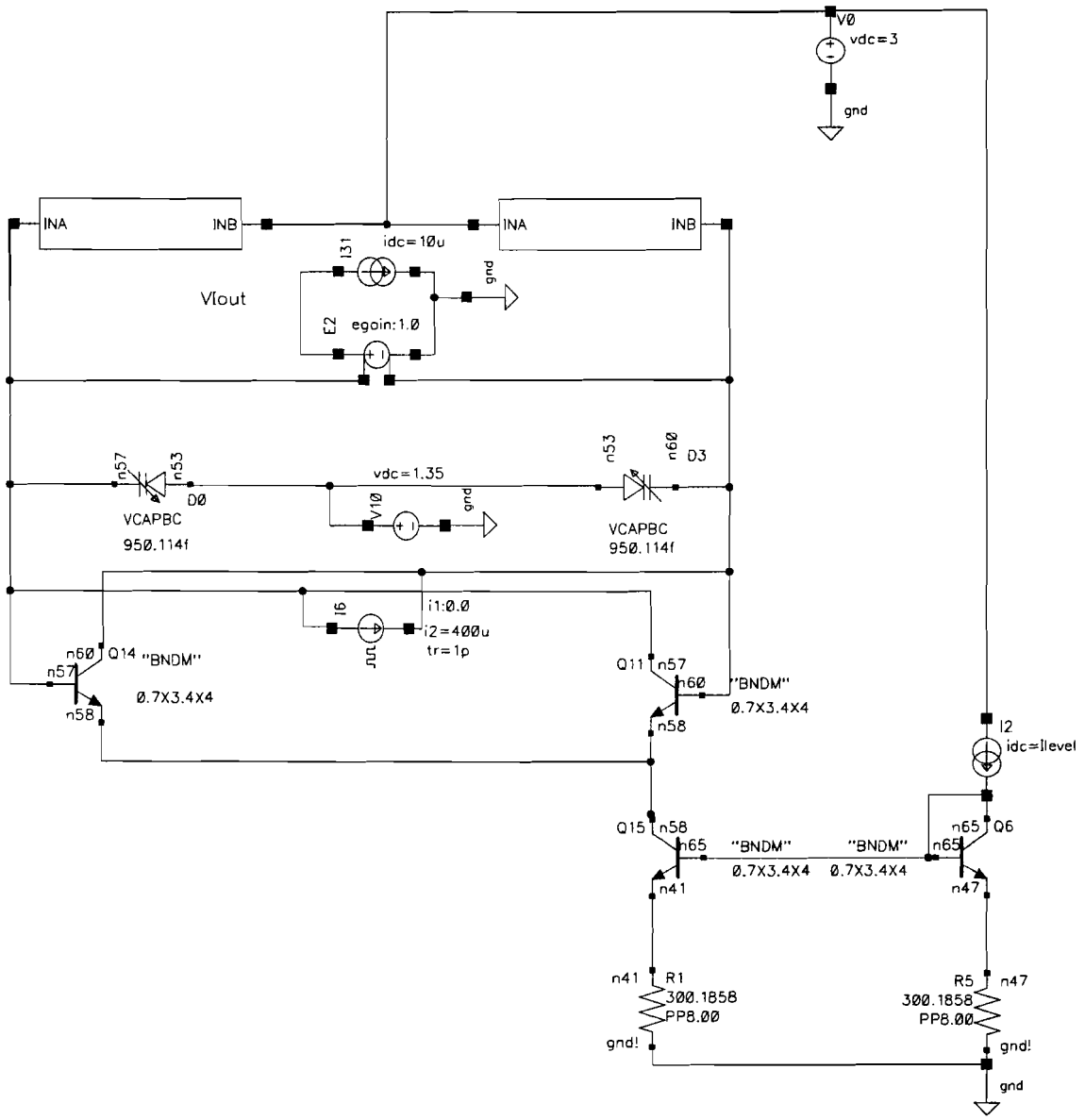

Figure 48: LC single-phase oscillator